Measures of complexity and entanglement in many-fermion systems

Aurel Bulgac, Matthew Kafker, and Ibrahim Abdurrahman
Department of Physics, University of Washington, Seattle, Washington 98195-1560, USA

(Received 9 March 2022; revised 14 June 2022; accepted 4 April 2023; published 26 April 2023)

There is no unique and widely accepted definition of the complexity measure (CM) of a many-fermion wave function in the presence of interactions. The simplest many-fermion wave function is a Slater determinant. In shell-model or configuration interaction (CI) and other related methods, the state is represented as a superposition of a large number of Slater determinants, which in the case of CI calculations reaches about 20 billion terms [Johnson, arXiv:1809.07869]. Although in practice this number has been used as a CM for decades, it is ill defined: it is not unique, and it depends on the particular type and the number of single-particle wave functions used to construct the Slater determinants. The canonical wave functions and/or natural orbitals [Löwdin, Adv. Phys. **5**, 1 (1956); Löwdin and Shull, Phys. Rev. **101**, 1730 (1956); Bardeen *et al.*, Phys. Rev. **108**, 1175 (1957); N. N. Bogoljubov, Il Nuovo Cimento **7**, 794 (1958); Valatin, Il Nuovo Cimento **7**, 843 (1958); de Gennes, *Superconductivity of Metals and Alloys* (CRC Press, Boca Raton, FL, 1999); Ring and Schuck, *The Nuclear Many-Body Problem*, 1st ed. (Springer-Verlag, Berlin, 2004)] and their corresponding occupation probabilities are intrinsic properties of any many-body wave function, irrespective of the representation, and they provide a unique solution to characterize the CM. The non-negative orbital entanglement entropy, which vanishes for a Slater determinant, provides the simplest CM, while a more complete measure of complexity is the entanglement spectrum. We illustrate these aspects in the case of a complex nonequilibrium time-dependent process, induced nuclear fission described within a real-time density functional theory framework extended to superfluid systems, which can describe simultaneously the long-range and the short-range correlations between fermions. The orbital entanglement entropy of the fissioning nucleus illustrates the localization mechanism of the many-body wave function in Fock and/or Hilbert space. The (minimal) number of Slater determinants required to represent such a complex many-body wave function with a well-defined number of particles in the case presented here is about 10^{500}. The realistic case of the highly nonequilibrium nuclear fission process illustrated here is equivalent to a system of 23.328×10^9 interacting quantum spin-1/2 particles, a very large system for the study of quantum entanglement.

DOI: 10.1103/PhysRevC.107.044318

I. INTRODUCTION

Only two years after Schrödinger [1] published his equation, the representation of the wave functions for an interacting many-body system became a question of major concern. For a system of N spinless particles in three dimensions such a wave function would require $(n_s^3)^{N-1}$ complex numbers, where n_s is the number of discrete spatial points in one dimension. The smallest spatial separation between two spatial lattice points l determines the maximum momentum cutoff $\Lambda = \pi\hbar/l$. The simplest solution suggested almost a century ago for a system of many fermions was to use the Hartree-Fock (HF) approximation [2–5] and its later extension, the Hartree-Fock-Bogoliubov (HFB) approximation [6–10], which in three dimensions and in the absence of any symmetry is still numerically challenging even nowadays. At the same time, short-range correlations (SRCs) are critical in obtaining *ab initio* accurate descriptions of many-fermion systems. In the case of the dynamics of many-fermion systems out of equilibrium this is still a question which awaits to be fully addressed microscopically [11].

For fermion systems the elementary building block in constructing a many-fermion wave function is the Slater determinant, also known as the HF wave function. In the presence of pairing correlations the generalized Slater determinant, the HFB many-body wave function, plays a similar role, and often in the case of nuclei it requires a particle projection. Despite the short-range and strong character of the interactions between nucleons, many single-particle and collective properties of nuclei can be calculated quite successfully using mean-field theory approaches such as HF and HFB, Landau-Migdal theory for Fermi liquids, shell-model calculations, etc. In all these approaches a rather limited number of single-particle orbitals are typically used. When pairing correlations are present the Fermi surface is diffuse and the number of single-particle orbitals needed in order to describe the nuclear masses and the low-energy excited states in most applications is at most about twice as large as the total particle number [10,12].

For decades in nuclear physics the correlations have typically been treated with rather low-momentum cutoffs Λ and their effects have been rolled into effective (not always synonymous with accurate), mostly phenomenological, low-energy interactions. The typical argument used in calculations of open-shell nuclei was that the energy of the ground state converged quite rapidly as a function of the chosen cutoff. This is expected in the case of a variational approach, since errors of order $\mathcal{O}(\delta)$ in the many-body wave function lead to

errors $\mathcal{O}(\delta^2)$ in the energy near the minimum. Anderson [13], in discussing the treatment of electronic systems, characterized this kind of situation as the "quantum chemists' fallacy no. 1 and 2," of which even Wigner was partially guilty, as "you may get pretty good energetics out of a qualitatively wrong state." The perfect example is the case of a superconductor, in which, despite the fact that the contribution to the ground-state energy from the condensation energy is practically negligible, meaning the ground-state energy can be evaluated with sufficient accuracy in the absence of pairing correlations, the wave function with pairing correlations leads, however, to qualitative changes, which otherwise would have been completely overlooked.

The Slater determinants form a complete set of N-particle many-body states. The number of Slater determinants in an expansion of a many-fermion wave function has a very strong dependence on the size of the single-particle (HF) basis set. In configuration interaction (CI) or shell-model calculations [14], which are used to construct the ground state and a few excited states only, the dimension of the Hamiltonian matrix to be diagonalized, before any symmetry restrictions are imposed, is

$$\frac{N_{sp}!}{N!(N_{sp}-N)!} \approx \left(\frac{N_{sp}}{N}\right)^N, \quad \text{typically} \ll \left(n_s^3\right)^{N-1}, \qquad (1)$$

where N_{sp} is the size of the adopted single-particle Hilbert space. Notice that N_{sp} is the only adjustable parameter in Eq. (1) for a given particle number N. Similar arguments apply also for other many-body techniques such as coupled cluster approaches, the generator coordinate method, and certain implementations of the quantum Monte Carlo method. Does this number accurately describe the complexity of a CI many-body wave function? In the case of time-dependent processes it is well known that the dynamics are governed in general by statistical factors, namely, by the number of accessible states available for the system to evolve into for ergodic systems. As a result, underestimating the number of basis states could lead to inaccurate results, while overestimating this number can lead to unnecessary calculations. However, equilibration times might be significantly longer than specific characteristic times, in which case statistical arguments are not applicable.

The main questions we address in this work are the following:

(i) Does a useful measure or measures of the complexity of a many-body wave function exist?
(ii) Does a minimal set of N_{sp} single-particle states exist and what are its properties? This question received an answer many years ago [15–19].
(iii) How can one construct such a basis set easily?
(iv) Does a measure or measures of complexity of a many-body wave function shed any new light on nonequilibrium processes, where (local) thermalization has not had enough time to occur?

More than 70 years ago Levinger [20] invoked the quasideuteron model and the short-range character of the proton-neutron correlations in order to describe the nuclear photoeffect. Using realistic nucleon interactions, various authors observed that very-high-momentum single-particle states are occupied with significant probability [21,22]. As in the case of Levinger's quasideuteron model, the presence of the SRCs, reflected in the significant single-particle probabilities of high-momentum states, were crucial in order to describe the results of the $(e, e'p)$ experiments [23,24], which showed that deep single-particle levels were occupied with an unexpectedly low probability [22,25], $n_{sp} \approx 0.6$. Brueckner's framework was a parallel approach favored for decades [26,27] and used to include, although not explicitly, the role of SRCs in the mean-field treatment nuclei.

There is a rather wide range of observables that cannot be reproduced accurately in calculations in mean-field-type of treatments. One example is the nucleon momentum distribution, which has been studied theoretically and experimentally in cold-atom and nuclear systems for a long time [21–25,28–44], confirming Tan's [45–47] prediction made for systems with zero-range interactions that the high-momentum distribution behavior $n_k = C/k^4$ is in fact a generic feature of strongly interacting many-fermion systems, and thus a qualitative and quantitative feature of such systems both in and out of equilibrium. The important conclusion of many studies of nuclear systems was that approximately 20% of the spectral strength is found for momenta $k > k_F$.

In current studies of the masses and low-energy spectra of nuclei the role of SRCs is captured in a reduced space of single-particle orbitals using renormalization group techniques [48,49], and the SRCs never appear explicitly. Tropiano *et al.* [50,51] demonstrated recently how Levinger's quasideuteron model and the effect of SRCs on the nucleon momentum distribution can be reproduced at a low-momentum resolution using the similarity renormalization group (SRG) approach [48,49]. Within the SRG approach the scattering properties and energy spectra of very light nuclei are reproduced with impressive accuracy, although the quality degrades with increasing atomic mass [52], likely due to a simpler theoretical treatment of SRCs at only the next-to-next-to-leading-order level [53]. However, the simplification provided by the SRG approach in calculating ground-state and low-energy excited-state properties results in a rather complex and opaque structure of various observables, in particular the nucleon momentum distribution, which become complex many-body operators with the result that "the best choice of scale may not be so clear for analyzing SRC experiments because of the tradeoffs" [50]. The extension of the SRG approach to time-dependent nonequilibrium phenomena is yet to be realized. The dynamics are controlled by gain and loss in the case of kinetic equations, and therefore by the availability of final states in particular. Then, it is not obvious whether that SRG approach, which operates in a limited single-particle space, could describe time-dependent phenomena, such as fission or many-nucleon transfer reactions in heavy-ion collisions. Many outstanding issues, concerning the relevance of the SRCs in low-energy nuclear physics in particular, remaining to be addressed in the near future were discussed in recent papers [54,55]. As Miller [56] notes, the three scales

relevant to low-energy nuclear physics—size of nuclei, average separation between nucleons, and the nucleon size—are basically of the same order of magnitude, and thus there is effectively no scale separation and the effects of SRCs can be measured [57].

In Secs. II and III we describe the general properties of the canonical wave functions, which are needed to evaluate the canonical occupation probabilities and the orbital entanglement entropy, which provide measures of the complexity and of the many-body wave functions. The complexity of a many-body wave function can be characterized by the degree of nonsimilarity to a Slater determinant. Canonical wave functions were introduced a long time ago, in connection with describing pairing correlations, as the eigenvectors of the one-body density matrix. The mathematical framework for describing superfluid fermionic systems was formulated in terms of quasiparticles by Bogoliubov [7] and Valatin [8]. Zumino [58] and Bloch and Messiah [59] showed that one can introduce a particular set of quasiparticles, with similar properties to the set used by Bardeen *et al.* [6] (BCS), the canonical set of states (see also Ref. [10]). Löwdin [15], Löwdin and Shull [16] introduced the natural spin orbitals as the eigenvectors of the one-body density matrix. The definitions of the canonical wave functions and the natural orbitals are mathematically identical, yet have been used in different contexts, particularly extensively in chemistry [19], but lately also in nuclear physics [60–73], often without realizing that they represent the same complete set of orthonormal single-particle orbitals, namely, the canonical set of states.

It has been proven that if one intends to represent a correlated many-body wave function as a sum over Slater determinants, the natural orbitals or, in other words, the canonical wave functions set is the optimal set, namely, the smallest-size single-particle basis set [15–19]. Mathematically it is obvious that the canonical wave functions or the natural orbitals form a full orthonormal set, but as far as we can judge from the literature many properties of this set were never studied, as only a small reduced number of canonical wave functions was ever extracted numerically and only some properties of this reduced set were discussed. We show here that the canonical wave functions have some very distinctive, even striking and peculiar, properties which were never discussed in literature.

We demonstrate that the canonical wave functions are basically of three types: (i) a subset similar to usual mean-field single-particle wave functions; (ii) a subset of wave functions corresponding to occupation probabilities $n_k \approx C/k^4$, which oscillate much faster than the mean-field type of single-particle wave functions, are fully localized inside the system, have rather small occupation probabilities, and are typically ignored in evaluation of the ground-state properties of nuclei; and (iii) a subset of canonical wave functions localized outside the system and which play an insignificant role in defining physical properties of the system. The first subset has a size comparable to the particle number. The size of the second subset, not explicitly discussed in literature, is typically an order of magnitude larger in size than the first subset (or even larger for small spatial resolutions) and its size is determined by the level of spatial resolution adopted or the momentum cutoff

$$\Lambda = \frac{\pi\hbar}{dx}, \tag{2}$$

which is defined by the adopted spatial resolution $dx = l$. Only canonical wave functions of types (i) and (ii) are relevant in order to accurately evaluate properties of a many-body system and in particular SRCs and the entanglement or the Boltzmann and Shannon entropies. We will show that the combined number of states of types (i) and (ii) is approximately given by phase space volume

$$g\frac{4\pi}{3}r_0^3 A\frac{4\pi}{3}\Lambda^3\frac{1}{(2\pi\hbar)^3} = \frac{8\pi^2}{9}\left(\frac{r_0}{dx}\right)^3 A, \tag{3}$$

where $g = 4$ is the spin-isospin degeneracy factor and $r_0 = 1.2$ fm for nuclei. In Sec. IV we discuss the definition of the orbital entropy for a system of indistinguishable particles.

In Sec. V we illustrate the insight the time evolution of the entanglement or Boltzmann entropy can provide in the case of quantum nonequilibrium processes, specifically induced nuclear fission, and demonstrate that the entanglement entropy and therefore the size of the physically relevant canonical set has a nonmonotonic time dependence, of similar origin as the widely discussed many-body localization in one-dimensional (1D) systems [74–89]. In the dynamics of isolated systems the evolution of the entanglement entropy plays the role of thermodynamic entropy for local observables [90–92]. The manner in which the case of induced fission is described theoretically is similar to what in the condensed matter literature is called quenching, when a system is prepared as the stationary state of a nuclear Hamiltonian subject to external constraints and then it is evolved in time under a pure Hamiltonian with no constraints. The realistic case of the highly nonequilibrium nuclear fission process illustrated here is equivalent to a system of $8 \times (N_x N_y N_z)^2 = 8 \times (30^2 \times 60)^2 = 23.328 \times 10^9$ interacting quantum spin-1/2 particles. This nuclear system is likely by orders of magnitude the largest system where quantum entanglement has been studied so far in literature.

The experience gathered during more than a decade of studying nonequilibrium processes in nuclear systems and cold-atom systems seem to point towards a rather unexpected emerging scenario. It was demonstrated that pairinglike correlations can emerge at very large excitation energies, when they are not supposed to exist [93–97]. One can partially understand such behavior using the semiclassical Nordheim [98] and Boltzmann-Uehling-Uhlenbeck [99] approach to quantum kinetic phenomena, which was recently extended in a pure quantum framework [11]. The neutron-neutron and proton-proton collisions are captured in a time-dependent extension of the density functional theory (DFT) [95,100] by including the pairing field. As we will demonstrate here, as well in the case of induced fission (see Ref. [11] and Sec. V), the time-dependent pairing fields lead to a large population of high-momentum single-particle states, a process which is expected in nonequilibrium phenomena, as systems typically evolve towards large regions of allowed phase space. We present our conclusions in Sec. VI.

II. THE CANONICAL BASIS OR NATURAL ORBITAL SET

We show here how using the canonical [10] (introduced for treating superfluid systems) or natural orbital [15,16] basis set one can get insight into how many single-particle states are needed to accurately describe various properties of a physical system.

As the single-particle strength is spread by interactions over a wide energy interval the structure of the many-body wave function is always very complex. Even in a reduced single-particle Hilbert space, as used in shell-model calculations, the number of contributing Slater determinants is of the order of tens of billions [14], a number which depends very strongly on the type of the single-particle set of wave functions used. This number is only optimal if one uses the canonical or natural orbital set [15–19]. The complexity can be quantified for any quantum state $|\Phi\rangle$ by evaluating the orbital entanglement or quantum Boltzmann one-body entropy [11,66,98,99,101–107]

$$S = -g \sum\!\!\!\!\!\!\int_k n_k \ln n_k - g \sum\!\!\!\!\!\!\int_k [1-n_k]\ln[1-n_k], \tag{4}$$

where g is the spin-isospin degeneracy, $\sum\!\!\!\!\!\!\int$ implies summation over discrete and integration over continuous variables, respectively, and n_k are the canonical occupation probabilities

$$\int d\zeta\, n(\xi,\zeta)\phi_k(\zeta) = n_k\phi_k(\xi), \quad 0 \leqslant n_k \leqslant 1, \tag{5}$$

$$\sum\!\!\!\!\!\!\int_\xi \phi_k^*(\xi)\phi_l(\xi) = \delta_{kl}, \tag{6}$$

$$N = \sum\!\!\!\!\!\!\int_k n_k, \tag{7}$$

where N is the total particle number and $n(\xi,\zeta)$ is the number density matrix defined accordingly[1]:

$$n(\xi,\zeta) = \langle\Phi|\psi^\dagger(\zeta)\psi(\xi)|\Phi\rangle. \tag{8}$$

Here $\psi^\dagger(\xi)$ and $\psi(\xi)$ are the field operators for the creation and annihilation of a particle with coordinate $\xi = (\boldsymbol{r},\sigma,\tau)$ (spatial, spin, and isospin coordinates) and $|\Phi\rangle$ is an arbitrary quantum many-body state, either static or time dependent. The wave function Φ can describe either a static or time-dependent many-body system, and therefore the canonical occupation numbers and the corresponding canonical wave function can be time dependent as well.

The many-body wave function Φ can be a member of a Hilbert space, if the particle number is well defined, or of the Fock space, in which case it will contain components with different particle numbers. We will discuss here both cases in the context of nuclear fission. The one-body density $n(\xi,\zeta)$ can also be defined as [15–17,19]

$$n_N(\xi_1,\ldots,\xi_N,\zeta_1,\ldots,\zeta_N) = \Phi(\xi_1,\ldots,\xi_N)\Phi^*(\zeta_1,\ldots,\zeta_N), \tag{9}$$

$$n(\xi,\zeta) = N\int\prod_{k=2}^{N} d\xi_k n_N(\xi,\xi_2,\ldots,\xi_N,\zeta,\xi_2,\ldots,\xi_N). \tag{10}$$

The orbital entanglement entropy S defined in Eq. (4) is nonvanishing in the ground state of any interacting system [11,66,101,106,109], unlike the textbook thermodynamic entropy. The orbital entanglement entropy S attains its minimum value in the case of a pure Slater determinant $S_{\min} = 0$, when $n_k \equiv 1$ or $n_k \equiv 0$, and its maximum value when $n_k \equiv N/N_{sp}$, where N_{sp} is the dimension of the single-particle space and the single-particle strength is spread uniformly over the entire Hilbert space. The entropy S, which is thus a measure of the complexity of the many-body wave function, can be evaluated accurately only when very-high-momentum occupation probabilities up to values $n_k \approx 10^{-6}$ are taken into account (see Sec. V).

From a quantum information science (QIS) point of view it is convenient to use the Shannon definition of the entropy [108], and use instead a rescaled set of canonical occupation probabilities (typically arranged in decreasing order)

$$\tilde{n}_k = \frac{n_k}{N}, \quad \sum\!\!\!\!\!\!\int_k \tilde{n}_k = 1, \quad 0 \leqslant \tilde{n}_k \leqslant \frac{1}{N}, \tag{11}$$

$$\overline{S} = -\sum\!\!\!\!\!\!\int_k \tilde{n}_k \log_2 \tilde{n}_k = -\frac{1}{N}\sum\!\!\!\!\!\!\int_k n_k \log_2 n_k + \log_2 N. \tag{12}$$

In the case of Fermi systems the minimum and maximum possible values of the Shannon entropy are

$$\overline{S}_{\min} = \log_2 N, \quad \overline{S}_{\max} = \log_2 N_{sp}. \tag{13}$$

The minimum value for $\overline{S}$ is achieved only in the case of a Slater determinant for $N > 1$ particles, and for any superposition of Slater determinants, $\overline{S} > \log_2 N$.

Both entropies S and $\overline{S}$ obviously characterize the level of complexity of the many-body wave function: the extent to which particle interactions spread the single-particle strength over the entire spectrum. It is important to notice that both entropies can attain their minimum values for states which as a rule do not correspond to a minimum total energy. Basically both of these entropies characterize, in slightly different manners, the degree of the entanglement of the many-body system and henceforth we will use only the Boltzmann entropy S from this point onwards.

III. PROPERTIES OF THE CANONICAL WAVE FUNCTIONS

The canonical states or the natural orbitals $\phi_k(\xi)$ form a complete set

$$\sum\!\!\!\!\!\!\int_k \phi_k(\xi)\phi_k^*(\zeta) = \delta(\xi-\zeta). \tag{14}$$

Since $n(\xi,\zeta)$ basically vanishes when either spatial coordinate is well outside the system, any function $f(\xi)$ with support outside the system is automatically an eigenstate of

[1]Some authors prefer the definition of the density matrix normalized to 1 [17,108], instead of particle number N, as in this case the space of density matrices becomes convex.

$n(\xi,\zeta)$ with $n_k \approx 0$. The canonical states in the case of a finite nucleus in vacuum form a set with cardinality $\mathfrak{c}$, the cardinality of $\mathbb{R}^3$. If the nucleus is simulated in a finite box then the number of canonical states is countable and the set has the cardinality $\aleph_0$, the cardinality of the integers. Since for a stable nucleus the number density decays exponentially at large distances, the description of a bound nucleus in a sufficiently large simulation box should be sufficient, and a smaller set of single-particle wave functions with cardinality $\aleph_0$ should always suffice.

An eigenfunction $\phi_k(\xi)$ with $n_k > 0$ has its support largely inside the system, where the support of $n(\xi,\zeta)$ is, and one can presume that it oscillates with the maximum momentum $p_{\max} = \sqrt{2m|U|}$ that a typical nuclear mean field can support for a bound state, where $U \approx -50$ MeV is the depth of the mean field. One can then conjecture that the total number of states with $n_k > 0$ is of the order of the total number of bound quantum states a nuclear mean field can sustain,

$$N_{\max} \approx \frac{4\pi p_{\max}^3}{3}\frac{4\pi r_0^3 A}{3}\frac{1}{(2\pi\hbar)^3} \approx 0.5A, \tag{15}$$

where $r_0 = 1.2$ fm and A is the total number of nucleons, and where we did not account for spin and isospin degrees of freedom. (The spin-isospin degeneracy was not accounted for here.) Since both normal number and anomalous densities are constructed from canonical quasiparticle wave functions) qpwfs, with strictly nonvanishing occupation probabilities $0 < n_k \leqslant 1$, it then follows that only a finite set of such functions is likely needed to represent the densities. We show below that Eq. (15) grossly underestimates the size of the canonical basis set with $n_k > 0$. Using Eqs. (A8) and (5) it follows that the density matrix $\overline{n}(\xi,\zeta)$ has the same eigenfunctions $\phi_k(\xi)$:

$$\int d\zeta\, \overline{n}(\xi,\zeta)\phi_k(\zeta) = (1-n_k)\phi_k(\xi). \tag{16}$$

This equation may be used to construct the canonical states localized mostly outside the system.

One can introduce the time-reversal canonical orbitals [12], not necessarily identical to those defined in Eq. (A22),

$$\phi_{\overline{k}}(\xi) = i\sigma_y\phi_k^*(\xi), \tag{17}$$

where σ_y is the Pauli matrix.

We first illustrate the properties of the canonical wave functions with some generic numerical results obtained for a one-dimensional example, which retains all the qualitative features of a three-dimensional system. For the sake of simplicity we have chosen a one-dimensional system with potential and pairing fields

$$V(x) = \frac{V_0}{1+\frac{\cosh(x/a)}{\cosh(R/a)}}, \tag{18}$$

$$\Delta(x) = \frac{\Delta_0}{1+\frac{\cosh(x/a)}{\cosh(R/a)}}, \tag{19}$$

where we use the notation for the spatial coordinate $-\infty < x < \infty$, $V_0 = -50$ MeV, $\Delta_0 = 3$ MeV, $R = r_0 A^{1/3} = 14.9$ fm, $a = 0.5$ fm, and $\mu = -5$ MeV. (We avoid using a Woods-Saxon potential well in order not to generate singularities of the derivatives of the wave functions at the origin, which would lead to unphysical long momentum tails of the wave functions.) We solved the non-self-consistent superfluid local density approximation (SLDA) or HFB equations for the qpwfs [96,110], using the discrete variable representation (DVR) method [111],

$$\begin{pmatrix} H-\mu & \Delta \\ \Delta & -H+\mu \end{pmatrix}\begin{pmatrix} \mathrm{u}_k \\ \mathrm{v}_k \end{pmatrix} = E_k\begin{pmatrix} \mathrm{u}_k \\ \mathrm{v}_k \end{pmatrix}, \tag{20}$$

in a box of size $L = 80$ fm and with four different lattice constants $dx = 1, 0.5, 0.25, 0.125$ fm, where

$$H = -\frac{\hbar^2}{2m}\frac{d^2}{dx^2} + V(x) \tag{21}$$

and m is the nucleon mass, in the absence of spin-orbit interaction. Equations (20) are for the components $\mathrm{u}_k(x)$ with spin up and $\mathrm{v}_k(x)$ with spin down. The equations for the components $\mathrm{u}_k(x)$ with spin down and $\mathrm{v}_k(x)$ with spin up are obtained from these equations by changing the sign of the pairing field $\Delta(x)$ only [96,110]. The SLDA equations for cold fermionic gases and nuclei have the same structure in this case. It is straightforward to extend this type of analysis to more complicated geometries, for example, the pasta phase in neutron star crusts, or the superconductor–normal metal–superconductor (SNS) junctions in condensed matter physics. The case discussed here is equivalent to a NSN junction. This analysis equally applies to infinite periodic systems.

This one-dimensional model is equivalent to solving the SLDA equations for a spherical system, in this case for s orbitals, with orbitals $\phi_k(x) = -\phi_k(-x)$ and $x \geqslant 0$ in the present formulation. For a three-dimensional spherical system the wave functions would be $\psi(\boldsymbol{r}) = \phi(r)/rY_{lm}(\theta,\phi)$ and $r = x \geqslant 0$. For angular momenta $l > 0$ one has to add the centrifugal potential $\hbar^2 l(l+1)/2mr^2$. In the presence of the centrifugal barrier a classically forbidden region appears near the origin and some of the corresponding canonical wave functions for $l > 1$ will have the character of "exterior" functions with occupation probabilities n_k beyond the UV knee shown in Fig. 2. The one-dimensional normal number density $n(x)$ here is only for the fermions with spin down, which in the case of even fermion particle number is identical to the normal number density of the spin-up particles. As shown in Ref. [112] the anomalous density $\kappa(x)$ has longer exponential tails than the number density $n(x)$. This longer tail of the pairing field becomes particularly important as one approaches the nucleon drip line. This behavior should be also apparent in the profiles of $V(x)$ and $\Delta(x)$, an aspect which we neglected here and which does not change the qualitative behavior of these densities (see Fig. 1). Figure 1 also shows that with increasing spatial resolution ($dx \to 0$) the normal density is more accurately reproduced at larger distances. We have also checked that Eqs. (A20) and (A21) in the Appendix correctly reproduce the normal and anomalous densities when using the canonical wave functions. From the spatial behavior of the canonical wave functions illustrated in Figs. 3 and 4 it is obvious that they can be obtained with real accuracy using semiclassical quantization conditions, as they are almost perfect stationary standing waves in an almost perfect square well potential.

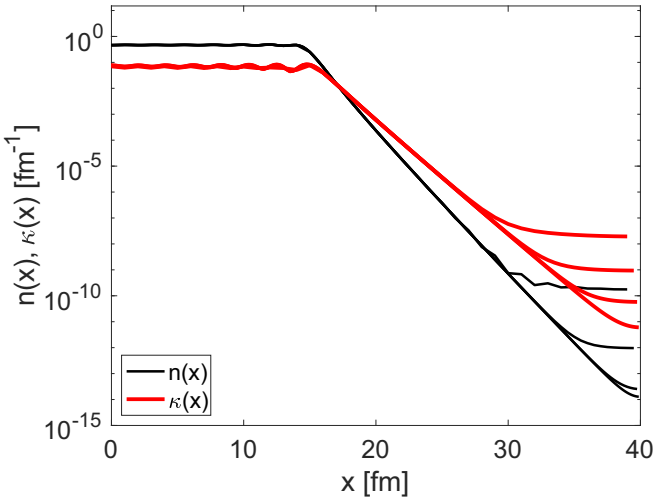

FIG. 1. The normal number (black) and anomalous (red) densities for $x \geqslant 0$, for four lattice constants in decreasing order $dx = 1$, 0.5, 0.25, 0.125 fm. $n(x)$ and $\kappa(x)$ stand for $n(x, x)$ and $\kappa(x, x)$, respectively.

The canonical occupation probabilities n_k shown in Figs. 1 and 2 have a conspicuous behavior not discussed previously in literature. For smaller lattice constant dx the maximum momentum cutoff $\Lambda = \hbar\pi/dx$ is large and the spectrum of n_k extends to high energies. The profile of n_k has two obvious "knees," one close to the Fermi level, the infrared (IR) knee, where a transition from the BCS-like behavior of n_k to a powerlike behavior occurs for $k \approx 20$ in Fig. 2, and a second one at a high energy, the ultraviolet (UV) knee. The canonical wave functions $\phi_k(x)$ have the expected spatial

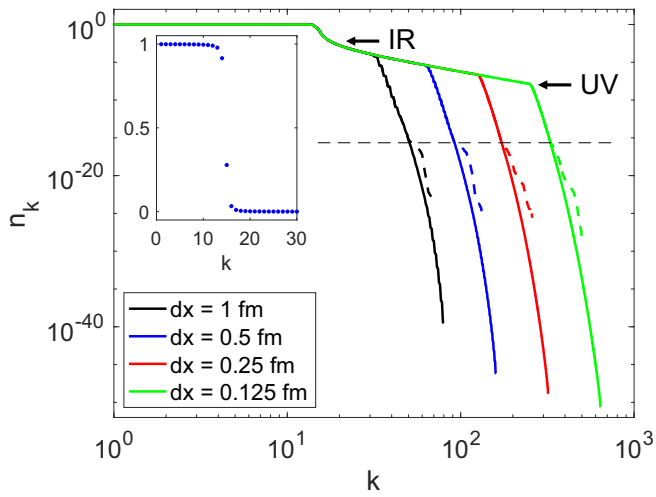

FIG. 2. The canonical occupation probabilities for four lattice constants dx in a log-log scale, corresponding to momentum cutoff $\Lambda = \pi\hbar/dx$. In the inset we plot n_k in the linear scale close to the Fermi surface. The results obtained with increased machine precision, 10^{-40}, are shown with continuous solid lines. The dashed horizontal black line shows the level of typical machine double precision, 10^{-16}, and dashed lines for n_k show the corresponding results obtained for the occupation probabilities.

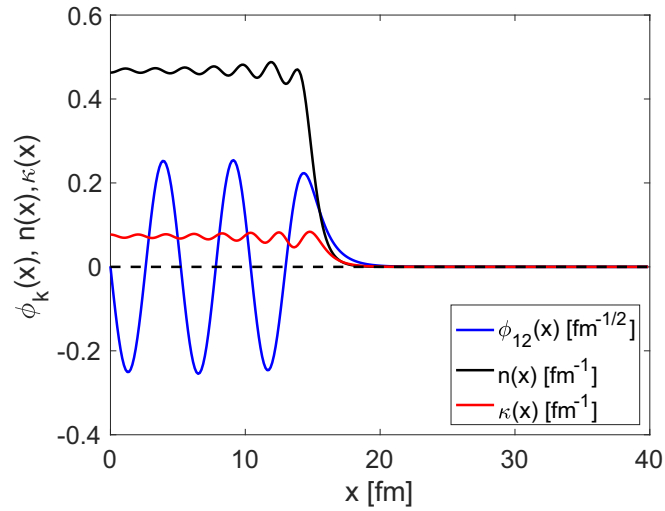

FIG. 3. The canonical wave function $\phi_{12}(x)$ and occupation probability $n_{12} = 0.978$ along with profiles of the number density $n(x)$ and of the anomalous density $\kappa(x)$ in the case $dx = 0.125$ fm. Since $V(x) = V(-x)$ and $\Delta(x) = \Delta(-x)$, all these functions have well-defined spatial parities and we represent these quantities only for $x \geqslant 0$.

behavior as long as their support is commensurate with the support of the number density matrix $n(x, y)$ as discussed above [see Eq. (5), the text below, and Figs. 3 and 4 in the case of $dx = 0.125$ fm]. However, as soon as the support of the canonical wave functions $\phi_k(x)$ is essentially outside the support of the density matrix $n(x, y)$ (see Fig. 5, for which the index k is on the right of the UV knee in Fig. 2), the corresponding n_k decay significantly faster with k. Both the profiles and the numerical values of n_k for these canonical states can be obtained with greater accuracy using increased precision (see Fig. 2). These canonical occupation probabilities do not identically vanish simply due to obvious quantum

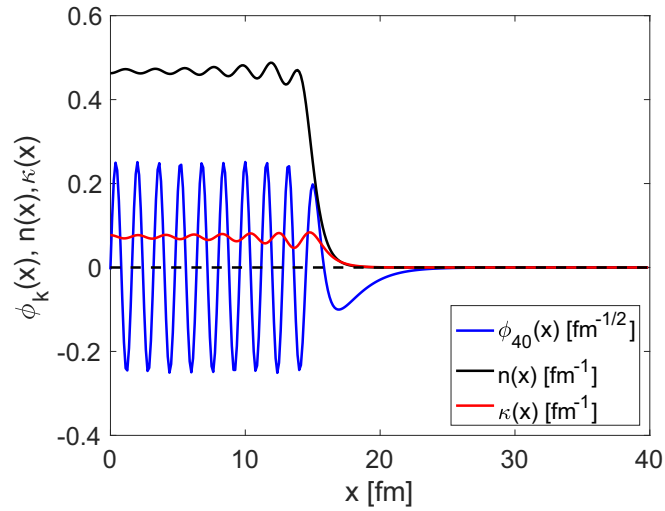

FIG. 4. The same as Fig. 3 for $\phi_{40}(x)$ and $n_{40} = 1.298 \times 10^{-4}$, localized inside the system, with k in the interval between the IR knee and the UV knee.

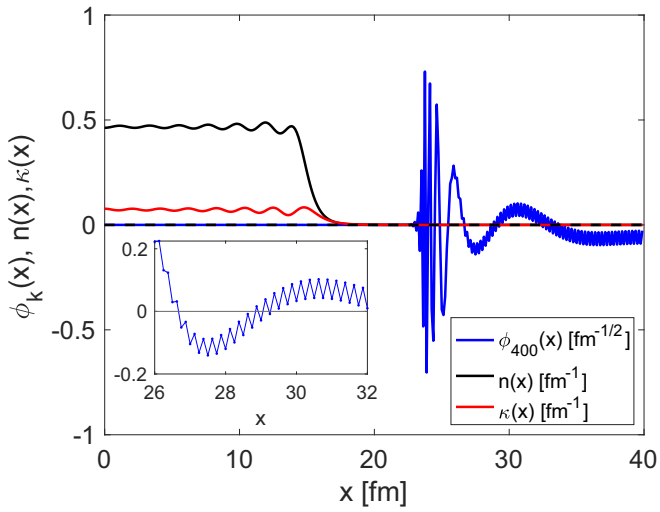

FIG. 5. The same as Fig. 3 for $\phi_{400}(x)$ and $n_{400} = 2.6 \times 10^{-13}$, an "exterior" canonical wave function localized outside the system, with k beyond the UV knee. These types of wave functions clearly cannot be solutions of a typical Schrödinger equation with a local potential. The inset shows that the high-frequency spatial oscillations have a wavelength $2dx$, determined by the momentum cutoff Λ. In the limit $\Lambda \to \infty$ these canonical wave functions have no spatial derivatives, as they oscillate from lattice point to lattice point.

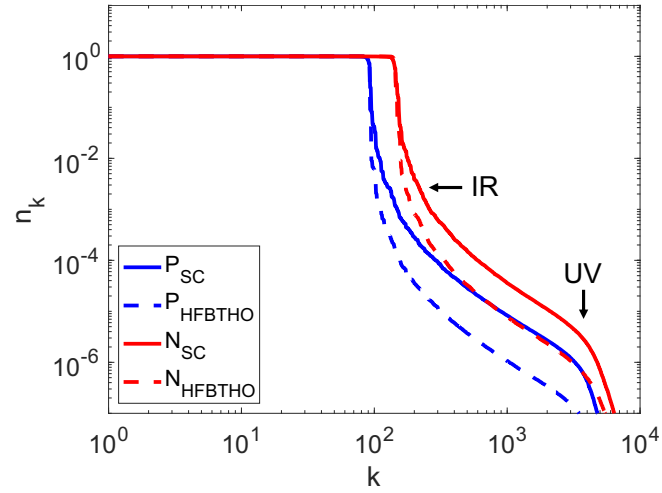

FIG. 6. The canonical occupation numbers at $t = 0$ obtained from HFBTHO and self-consistent SLDA solution on the three-dimensional spatial lattice for protons and neutrons, respectively, in the case of ^{236}U induced fission. Here n_k are ordered in decreasing order. The canonical occupation probabilities up to a constant define the entanglement spectrum $-\ln n_k$ [79].

localization effects, but they are increasingly smaller with increasing resolution and decreasing lattice constant dx. In the limit $dx \to 0$ the UV knee $\to \infty$ and at the same time the number of canonical states localized outside the system also tends to infinity. These nonlocalized canonical states, however, are irrelevant in describing the physical properties of the system.

Impact of long momentum tails in three dimensions

Below the IR knee in Figs. 2 and 6 the canonical occupation probabilities have the expected BCS behavior [6]. It is clear, however, that in between the IR knee and UV knee there is a region where the canonical occupation probabilities have a power-law behavior. Such a behavior, due to the short-range character of the nuclear forces, was predicted in 1980 by Sartor and Mahaux [28] and recently put clearly in evidence experimentally in nuclei by Hen *et al.* [36,43] and Cruz-Torres *et al.* [44]. Tan [46] has proven analytically the emergence of this behavior for fermions interacting with a zero-range interaction in three dimensions. Nuclear pairing is typically simulated in theory with a δ potential, which naturally leads to a local pairing field $\Delta(\xi)$ [112], similar to the case discussed here. Tan [46] showed that in the case of a zero-range interaction asymptotically $n_k \propto C/k^4$ for *any* many-body state. This power-law behavior of the number density is directly related to the divergence of the anomalous density matrix, Eq. (A7). In the case of a three-dimensional system it was shown in Ref. [112] that the anomalous density matrix $\kappa(\xi, \zeta) \propto 1/|\boldsymbol{r} - \boldsymbol{r}'|$ when $|\boldsymbol{r} - \boldsymbol{r}'| \to 0$, where $\boldsymbol{r}$ and $\boldsymbol{r}'$ are the spatial components of ξ and ζ, respectively.

It is also important to appreciate that the presence of the long momentum tail $n_k = C/k^4$ implies

$$\int_\Lambda^\infty dk k^2 n_k = \frac{C}{\Lambda}, \tag{22}$$

and therefore the particle number converges rather slowly as a function of the upper momentum cutoff Λ. The actual particle number can be reproduced in mean-field calculations simply by adjusting the chemical potential, thus introducing errors in the actual value of the chemical potential (a correction which might be small in practice). However, the total kinetic energy of a system

$$\int d^3k \frac{\hbar^2 k^2}{2m} n_k \tag{23}$$

obviously diverges if $\Lambda \to \infty$. Consequently, the correct evaluation of the total kinetic energy, and as a result the evaluation of the total energy of a many-body system, becomes a rather subtle problem, which in modern theoretical nuclear physics is resolved using the methods of effective field theory (EFT), where infinities are handled with "kid gloves." While within EFT one can define the total energy of the system, the separate definitions of either the kinetic, interaction, and even separate parts of the interaction energies become meaningless.

A closer analysis of Fig. 4 clearly shows that some canonical wave functions $\phi_k(x)$ oscillate much faster than the density $n(x, x)$. The oscillation of the number density $n(x, x)$ is due to confinement in a finite box, a finite Fermi momentum, and a relatively well-defined Fermi momentum k_F, and is a behavior known for decades for all finite Fermi systems. Our initial "naive" estimate of the maximum expected number of

relevant canonical wave functions [see Eq. (15)], is an underestimate, since the maximum momentum cutoff $\hbar\pi/dx > \sqrt{2m|U|}$. The coupling of the qpwfs components $v_k(\xi)$ to the continuum states, facilitated by $\Delta(\xi)$, leads to spatial oscillations with any wave vector up to the maximum allowed value $\hbar\pi/dx$. In the limit $dx \to 0$ the cardinality of the set of canonical wave functions $\phi_k(\xi)$ is either $\aleph_0$ for a finite system in a finite volume or $\mathfrak{c}$ for an isolated finite system in vacuum. Therefore, one should use, for the best estimate of the number $N_{\max}$, the cutoff momentum $p_{\max} = \hbar\pi/dx$, and from the condition of accommodating a standing wave in our "square well" potential, with $2R \approx 14.9$ fm in our numerical example, one obtains the approximate position of the UV knee at $k_{\max} = 2R/dx + \mathcal{O}(a/R) \approx 240$ for $dx = 0.125$ fm (as k counts the number of half wavelengths inside the potential well), in perfect agreement with our numerical identification of the UV knee in Fig. 2. When coupling a bound state through the pairing field Δ with the continuum, the strength of the bound state is spread over a large energy range with very long tails, with a Lorentzian shape of the spectral distribution [112]. Moreover, in time-dependent phenomena, even in the absence of a true pairing condensate (when the long-range order is lost) and at high excitation energies (with corresponding temperatures well above the pairing phase transition T_c) the remnant pairing field leads to many single-particle transitions and the quantum Boltzmann one-body entropy increases considerably [11].

With this in mind one can now provide a better estimate of the size of the canonical basis set for a three-dimensional system in a finite simulation box with sides of length $L_x = N_x dx$, $L_y = N_y dy$, $L_z = N_z dz$ ($dx = dy = dz$), ignoring spin and isospin degrees of freedom,

$$N_{\max} = \frac{4\pi}{3}\left(\frac{\hbar\pi}{dx}\right)^3 \frac{4\pi}{3} r_0^3 A \frac{1}{(2\pi\hbar)^3} = 2.2A\left(\frac{r_0}{dx}\right)^3. \quad (24)$$

At the same time the total number of single-particle quantum states in such a box is

$$N_{\text{spwfs}} = \frac{L_x L_y L_z}{(2\pi\hbar)^3}\left(\frac{2\pi\hbar}{dx}\right)^3 = N_x N_y N_z, \quad (25)$$

which is typically significantly larger. For example, for a typical simulation box for a heavy nucleus with volume 30^3 fm^3 and $dx = 1$ fm the total number of qpwfs (here ignoring spin and isospin degrees of freedom) is $N_{\text{spwfs}} = 27\,000 \gg N_{\max} \approx 3.8A < 1000$. This estimate is accurate only for some quantities, such as particle number and total energy (see Sec. IV).

The classification of the wave functions as "interior," as in Figs. 3 and 4, and "exterior," as in Fig. 5, depends on the momentum cutoff Λ, particularly when discussing the entropy of a quantum state (see Sec. IV), and less so when evaluating the total energy of a system. Various sizes of sets of the canonical wave functions, with k smaller than the IR knee, have been considered in the evaluation of the binding energies of nuclei [61–73] and they missed the long momentum tails discussed in this work and their relevance. Moreover, for unclear reasons, when diagonalizing the one-body density matrix these authors obtained negative canonical occupation probabilities, while it is obvious that the one-body density matrix is a non-negative definite Hermitian operator.

IV. THE ORBITAL ENTANGLEMENT ENTROPY FOR A SYSTEM OF IDENTICAL PARTICLES

There exist a number of approaches in the literature for the definition of the orbital entanglement entropy in the case of indistinguishable particles [113–117], which typically depend on the single-particle basis used. One can often find similar either explicit or implicit statements (see, e.g., Refs. [66,73]) that orbital entanglement entropy is basis dependent. This amounts to the statement that the orbital entanglement entropy corresponding to a many-body wave function depends on whether one uses harmonic oscillator wave functions or plane waves, for example. Since different choices would lead to different values of the orbital entanglement entropy it is not clear what would be the use of such a definition, as clearly it will not represent some intrinsic property of the many-body system. However, this dilemma is easily resolved if one realizes that, for an arbitrary many-body wave function, there is a unique definition of the single-particle orbitals, either the natural orbitals introduced by Löwdin [15], Löwdin and Shull [16] or the mathematically identical definition used to introduce canonical single-particle wave functions in the case of superfluid systems. These sets and the properties of the single-particle wave functions are basis independent and are uniquely defined by the many-body wave function. Together with the well-established mathematical proof due to Hohenberg and Kohn [118], a proof which withstood the test of time, that there is a one-to-one correspondence between the many-body wave function and the one-body density, and thus with the one-body density matrix, makes it obvious that the set of canonical wave functions or natural orbitals have an intrinsic value.

The introduction of the definition used in Refs. [113,114] for the orbital entanglement entropy was motivated by quantum computing applications, in which case one deals with well-defined single-particle orbitals corresponding to the specific physical realization of qubits, which are not necessarily the same as the needs of QIS. The information encoded in a many-body wave function is not identical to the information encoded in a specific representation of the same wave function in a chosen physical realization of a quantum computer. This is equivalent to the statement that the representation of a many-body wave function in terms of Slater determinants formed from single-particle wave functions is basis dependent.

The question of whether an arbitrary many-body wave function is representable either by the corresponding one-body density [118–121] or by its one-body density matrix [17,18] was discussed and resolved a long time ago. The definition of the one-body density matrix, Eq. (8), is valid for either a stationary or time-dependent many-body wave function $\Phi(t)$, with either well-defined particle number or not, and its representation through its eigenstates, here for the more general case of a time-dependent system, is invariant with respect to an arbitrary (time-dependent) unitary

transformation $\mathcal{U}(t)$:

$$n(\xi,\zeta,t) = \langle\Phi(t)|\psi^{\dagger}(\zeta)\psi(\xi)|\Phi(t)\rangle, \tag{26}$$

$$\int d\zeta\, n(\xi,\zeta,t)\phi_k(\zeta,t) = n_k(t)\phi_k(\xi,t), \tag{27}$$

$$n(\xi,\zeta,t) = \sum\!\!\!\!\!\!\int_k v_k^*(\xi,t)v_k(\zeta,t), \tag{28}$$

$$v_k^*(\xi,t) = \sqrt{n_k(t)}\phi_k(\xi,t), \tag{29}$$

$$\overline{v}_k^*(\xi,t) = \sum\!\!\!\!\!\!\int_l \mathcal{U}_{kl}(t)v_l^*(\xi,t). \tag{30}$$

In particular, the time-dependent HFB equations are invariant as well with respect to such unitary transformations. In other words, if at some time t the set of quasiparticle wave functions $v_k(\xi,t)$, $u_k(\xi,t)$ (see the Appendix) happens to be the canonical set, in general as time evolves the quasiparticle wave functions will not remain canonical [122]. The time-dependent number and anomalous densities are invariant with respect to such time-dependent unitary transformations [123], while the canonical occupation probabilities are always uniquely defined. Therefore, unlike the case of the stationary HFB equations, one cannot uniquely relate the quasiparticle wave functions with the eigenvalues of the corresponding HFB equations. This is a major difference with the Hartree-Fock problem, in both its time-dependent and stationary formulation. In the case of a time-dependent many-body wave function one should introduce at each time the instantaneous occupation probabilities $n_k(t)$ [see Eqs. (26) and (27)] in order to have a unique definition of the time-dependent orbital entanglement entropy $S(t)$:

$$S(t) = -g\sum\!\!\!\!\!\!\int_k n_k(t)\ln n_k(t) - g\sum\!\!\!\!\!\!\int_k [1-n_k(t)]\ln[1-n_k(t)]. \tag{31}$$

The usefulness of the orbital entanglement entropy becomes clear particularly in the case of nonequilibrium processes [74,80,83–85,124–126]. In the limit of a dilute and weakly interacting system the orbital entanglement entropy $S(t)$ becomes a very good approximation of the time-dependent nonequilibrium thermodynamic entropy of a many-body system [98,99], similar to the case of the classical Boltzmann equation (see discussion in Ref. [11]).

Using the definition of the orbital entanglement entropy through canonical or natural orbital occupation probabilities the HF many-body wave function always has a vanishing orbital entanglement entropy. The canonical or natural orbital occupation probabilities offer a natural, unique, and simple way to characterize the entanglement properties of systems of indistinguishable particles. As has been mathematically proven [17–19], using natural orbitals, an arbitrary many-body wave function has a well-defined and unique Schmidt decomposition, which thus allows a unique way to introduce the orbital entanglement entropy, irrespective of the single-particle basis used. The canonical or natural orbital occupation probabilities, which are obtained after the Schmidt decomposition of a many-body wave function, in order to construct the so-called entropy spectrum [79], can and do play a great role in characterizing topological phases of matter.

V. COMPLEXITY OF THE MANY-BODY WAVE FUNCTION IN THE CASE OF A NONEQUILIBRIUM PROCESS

Both the quantum Boltzmann one-body and Shannon entropies can be evaluated only after the evaluation of the canonical occupation probabilities [see Eqs. (4) and (12)]. Both these entropies reach their minimal values only in the case of pure Slater determinants. Only in the presence of interparticle interactions these entropies increase in value and can provide a measure of the complexity of the many-body wave function. As far as we are aware there exist no studies of how the complexity, or the degree of single-particle spreading over the entire spectrum, depends on real time in the case of a nonequilibrium process, particularly for a system with a high degree of complexity. Nuclear fission is a particularly interesting case and it provides an unexpected insight into how the many-body wave function evolves in time within the DFT framework from a state near the outer saddle point until after the two fission fragments are fully separated.

Nuclear fission is a typical example of a nonequilibrium quantum process and one would expect that the entropy would monotonically increase in time [11]. The actual situation, however, is more complex. We remind the reader that the entropy S defined in Eq. (4) is an entanglement entropy [66,101,106,109], which does not vanish even in the ground state of an interacting many-fermion system, unlike the thermodynamic entropy. In Fig. 12 we display the time dependence of the entropy $S(t)$ evaluated in several different manners, for initial conditions obtained in different methods and with and without particle number projection within DFT extended to superfluid systems [93,100,110,127–129]. We evaluate here the neutron and proton canonical occupation probabilities as a function of time, for both unprojected and projected total proton and neutron numbers, following the techniques described in Refs. [123,129], and illustrate the time evolution of the orbital entanglement entropy in the case of ^{235}U(n,f) induced fission with a low-energy neutron, described with the nuclear energy density functional SeaLL1 [130] and using the code LISE [131]. This extension of DFT to a superfluid fermion system, in the spirit of the local density Kohn-Sham framework, is called the time-dependent superfluid local density approximation (TDSLDA).

Beyond the UV knee, for the canonical states localized mostly outside the system, the mean kinetic energies ϵ_k drop in value and their contribution to the total kinetic energy is commensurate with what one expects from numerical discretization errors ($dx \neq 0$) of the continuum. As one can see from Fig. 7, in the region between the IR and UV knees (see Fig. 6), the canonical occupation probabilities have the approximate expected behavior $n_k \propto 1/\epsilon_k^2$, where

$$\epsilon_k = \langle\phi_k| - \frac{\hbar^2\nabla^2}{2m}|\phi_k\rangle. \tag{32}$$

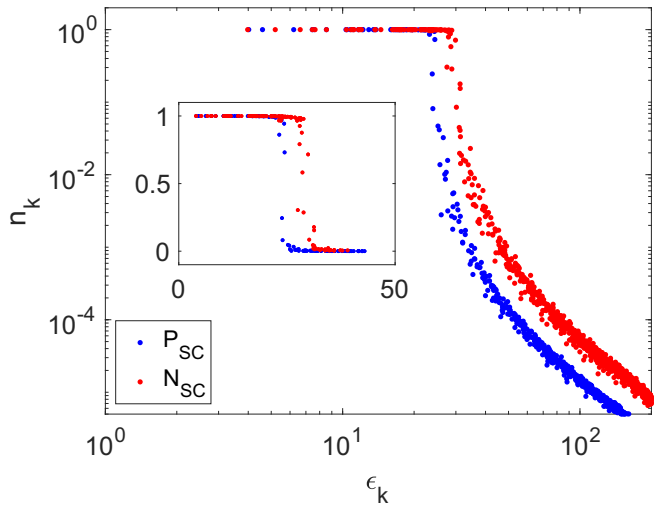

FIG. 7. The canonical occupation probability n_k as a function of ϵ_k. In the inset we show that the canonical occupation probabilities n_k around the Fermi level have the expected textbook behavior. Comparing Figs. 6 and 7 one sees that ϵ_k are only approximately monotonic functions of k, which, only for relatively large values of ϵ_k, can be related to eigenstates in the approximately square well nuclear self-consistent potentials for different angular momenta [132].

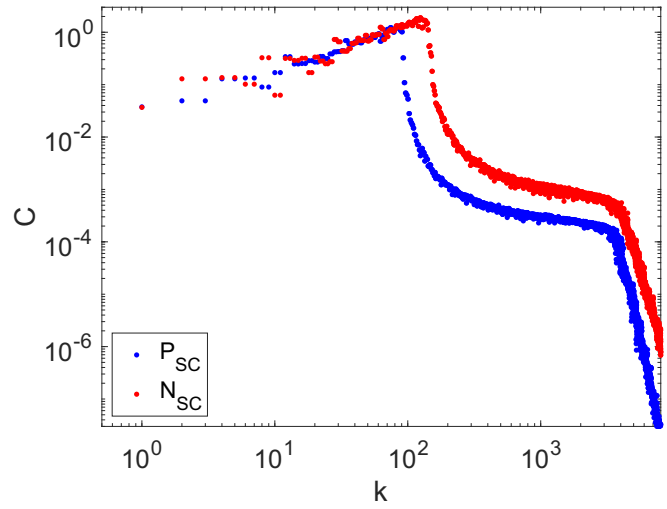

FIG. 8. The quantity $C = (2m\epsilon_k/\hbar^2)^2 n_k$, which in the regime $n_k \approx C/k^4$, between the IR and UV knees, defines Tan's contact.

Since nuclear systems are to a large extent saturating systems, while the linear momentum $\boldsymbol{p} = -i\hbar\nabla$ is not conserved, its absolute value is rather well defined and the single-particle wave functions can be well approximated in the semiclassical limit, the single-particle energies can be evaluated by quantization of classical orbits, and the shell structure of both spherical and deformed systems is reproduced with impressive accuracy [132].

As we have proceeded in all our past TDSLDA simulations of nuclear fission [95,96,133–135], the initial state was determined using the HFBTHO code [136,137] which uses a small single-particle set of wave functions of size, which is quite sufficient to estimate the total energy of a nucleus. Since the TDSLDA simulations are performed on a 3D spatial lattice $N_x N_y N_z = 30^2 \times 60$, with a lattice constant $l = 1$ fm, the size of the HFB matrix is much larger, $4 \times 30^2 \times 60 = 216\,000$, for neutrons and protons, respectively.

In Fig. 6 we show the canonical occupation numbers, up to the UV knee only, obtained using the HFBTHO self-consistent densities and a set of self-consistent solutions on the 3D spatial lattice at $t = 0$. If one is interested in the total particle number the sum $N = \sum_k n_k$ converges with an accuracy of 0.01 particles if summed up to $n_k \approx 10^{-5}$ (see below the discussion of Fig. 10), thus at most a few thousands of canonical states (both spin up and down) in the case of the self-consistent solution on the 3D spatial lattice, a number almost an order of magnitude smaller than the size of the basis set $2 \times 30^2 \times 60 = 108\,000$ (the factor 2 is for the spin).

Within the SLDA, or any treatment of pairing correlations with a local pairing field $\Delta(\xi)$, the theory requires regularization and renormalization [127,128]. We have checked that indeed

$$(\epsilon_k)^2 n_k \approx \left(\frac{\hbar^2}{2m}\right)^2 C \quad \text{if } k_{\rm IR} < k < k_{\rm UV} \tag{33}$$

(see Figs. 2, 6, 8), confirming the theoretical prediction of Refs. [28,46]. In the case of pure finite-range nucleon interactions, with no zero-range components, there is an upper momentum cutoff controlled by the interaction range. When treating nuclear systems as composed of proton and neutrons the typical momentum cutoff is $\Lambda \approx 600$ MeV/c, which is related to the QCD chiral symmetry breaking scale Λ_χ controlled by the nucleon size, as it makes no sense to consider the interaction between two nucleons when their quark clouds strongly overlap. Figure 8 demonstrates that between the IR and UV knees the canonical occupation probabilities approach asymptotically the expected behavior $n_k \propto 1/\epsilon_k^2$, even though our cutoff momentum $\Lambda = \hbar\pi/dx \approx 600$ MeV/c is not sufficiently high, as the momentum interval between the IR and the UV knees covers less than an order of magnitude. In this rather small momentum interval the behavior of the canonical occupation probability is closer to $n_k \propto 1/\epsilon_k^{2.3-2.5}$.

In the case of the HFBTHO solution the number of relevant canonical states is at most 1000 or so (see Fig. 9 for the number of canonical wave functions up to a given occupation number cutoff $n_\Lambda \approx 10^{-5}$). A particle projected many-body wave function can now be expressed as a sum of Slater determinants, built from canonical states and/or natural orbitals. The number of these Slater determinants can be considered as an appropriate measure of the complexity of a many-body wave function,

$$\frac{N_{CWFs}!}{N!(N_{CWFs}-N)!} \ll \frac{N_{sp}!}{N!(N_{sp}-N)!}, \tag{34}$$

which is exponentially smaller than the total number of possible Slater determinants (for either neutrons or protons) in the entire many-body Hilbert space corresponding to $N_{sp} = 2 \times N_x N_y N_z = 108\,000$. In the case of a shell-model or CI

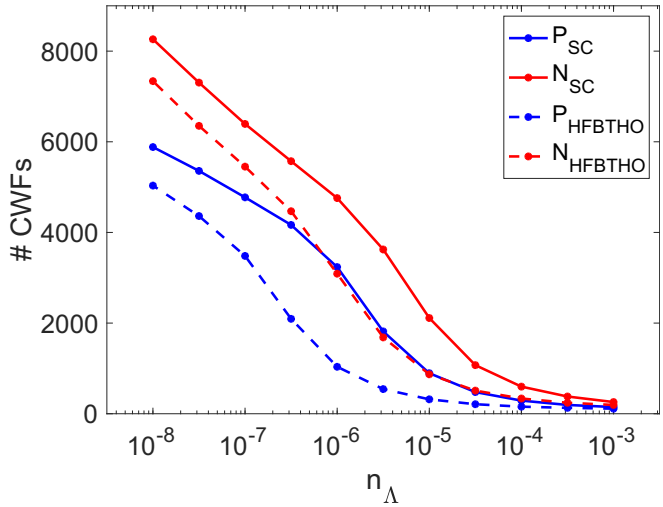

FIG. 9. The number of canonical wave functions at $t = 0$ as a function of the canonical occupation number cutoff n_Λ. The dashed lines correspond to the HFBTHO set of self-consistent solutions, while the solid line corresponds to the self-consistent solutions obtained on the 3D spatial lattice.

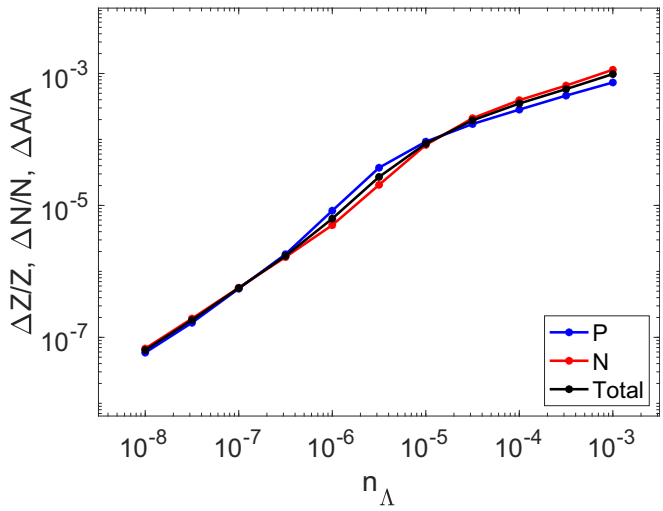

FIG. 10. The accuracy of the particle number evaluated for the self-consistent solutions at $t = 0$ as a function of the canonical occupation number cutoff.

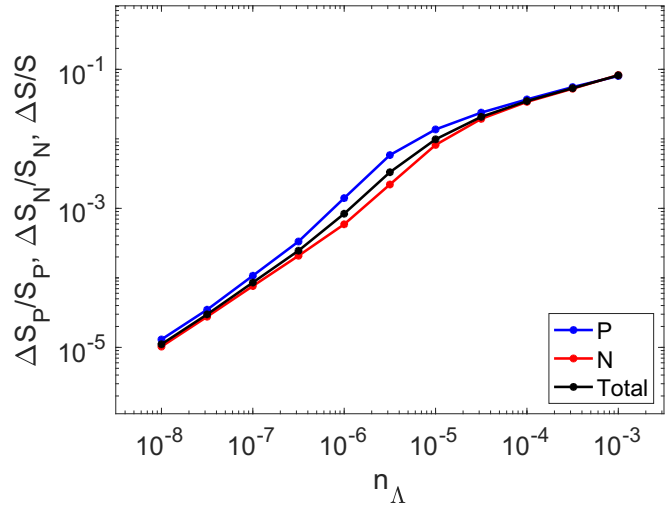

FIG. 11. The accuracy of the entropy evaluated for the self-consistent solutions at $t = 0$ as a function of the canonical occupation number cutoff.

calculation, for example, the complexity, and likely the accuracy as well, of the many-body wave function thus cannot be judged by the dimension of the many-body Hilbert space, which depends on the type of single-particle wave functions used.

In the case of HFBTHO the chemical potentials can be tuned to fix the desired particle numbers, even if the size of the single-particle space is (artificially) small. The particle number and the total energy of the system converge faster as a function of the cutoff in n_k when compared to the entanglement entropy $S(t)$ (compare Figs. 10 and 11). The lesson is that one cannot judge the quality or the complexity of a wave function by using a wave function obtained by a variational estimate for a qualitatively different observable (see also the arguments presented by Anderson [13] and our discussion above).

In a full TDSLDA simulation of fission we have extracted the canonical occupation probabilities as a function of time, and for all times their qualitative behavior is very similar to that at $t = 0$ as illustrated in Figs. 6 and 7, even though the pairing condensates are absent for times >700 fm/c and the role of SRCs is always manifest (see also Refs. [11,138]). The entropies $S(t)$ evaluated using HFBTHO initial wave functions are shown with the red solid and dashed lines in Fig. 12, in the case of unprojected particle numbers and projected particle numbers, respectively. The initial densities obtained with the code HFBTHO were placed on this spatial lattice and only the proton and neutron chemical potentials were slightly adjusted, in order to obtain the correct particle numbers $Z = 92$ and $N = 144$, respectively. Fully self-consistent initial wave functions obtained on the 3D spatial lattice $N_x N_y N_z = 30 \times 30 \times 60$ were used to determine the canonical occupation probabilities for the entropies $S(t)$ shown with black solid and dashed lines for unprojected particle numbers and projected particle numbers, respectively. The difference between the initial canonical occupation probabilities obtained using the HFBTHO, in which only the chemical potentials were adjusted, fully self-consistent solutions obtained on the 3D $N_x N_y N_z$ lattice are illustrated in Fig. 6. In Fig. 12 with dashed lines we present the corresponding entanglement entropies evaluated after the proton and neutron particle projections were performed at each time.

After each 100 fm/c the time-dependent neutron and proton density matrices were used to determine the instantaneous canonical occupation probabilities and evaluate the corresponding $S(t)$ shown in Fig. 12. To evaluate the entropy with an accuracy at the $\approx$0.1% level in Fig. 12 we needed to account for occupation probabilities with $n_k \geqslant 10^{-6}$. The entropies are larger in the case of particle unprojected wave functions, as such many-body wave functions have more

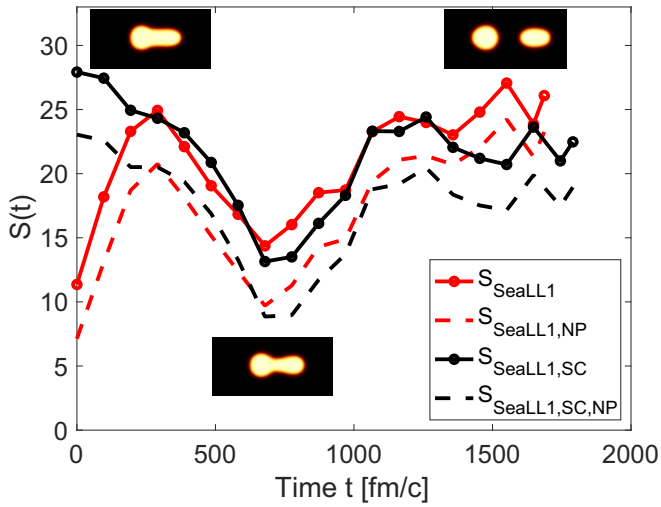

FIG. 12. The time dependence of the entropy $S(t)$ evaluated in the case of the induced fission of ^{235}U(n, f) with a low-energy neutron as a function of time from the vicinity of the outer saddle point until the two fission fragments are fully separated. The solid curves correspond to entropies evaluated without particle projection of the total many-body wave function, while the dashed curves are obtained after particle projection was performed before the canonical occupation probabilities were evaluated. The difference between the black and red curves is due to the difference between the initial states. In the case of the red curves we used initial densities obtained by solving the constrained self-consistent HFB equations using the code HFBTHO [136,137] using a relatively small set of transformed harmonic oscillator basis states. In the case of the black curves we obtained constrained self-consistent solutions directly on a 3D spatial lattice, which corresponds to a much larger single-particle space and a high momentum cutoff $\Lambda = \hbar\pi/l \approx 600$ MeV$/c$, where $l = 1$ fm is the spatial lattice constant and the dimension of the HFB matrix in this case is 216 000. Even though there are differences between the values of the entropies evaluated before and after a total particle projection was performed, the qualitative behavior of the quantum Boltzmann one-body entropy is by and large the same. The nuclear shapes obtained in TDSLDA during the time evolution are shown at 0, 675, and 1650 fm$/c$.

complexity, since they contain components with different particle numbers. At the same time, for the evaluation of the total particle number, and implicitly of the number densities and total energy of the system, it is sufficient to include only states with $n_k \geqslant 10^{-4}$. In time-dependent simulations, however, we have found that one cannot limit the number of qpwfs included in the calculations without severely affecting the outcome. A reformulation of the time-dependent DFT within a canonical wave-function basis set does not exist at this time. A major difficulty is that a set of initial canonical wave functions does not remain canonical under time evolution.

Our initial nuclear configuration corresponds to a nucleus slightly above the outer fission barrier, when the nucleus starts its evolution towards the scission configuration and the neck is formed. Scission occurs quite fast after a time $\approx$700 fm$/c$, after which the two fission fragments recede from each other, although their shapes still evolve and their equilibrium is attained at much later times [95,96]. The initial wave function describes the ground state of a shape-constrained nucleus, with thus technically zero thermodynamic many-body entropy. While the initial state was a "bound" state, the final nonstationary state lies in a continuum, where the density of many-body states is very large, even in the finite simulation box used in our numerical simulation.

In the case of HFBTHO initial conditions the entropy of the nucleus increases up to a time $t \approx 300$ fm$/c$, matching the entropy of the system obtained with fully self-consistent initial conditions obtained on the spatial lattice. Once the initial HFBTHO conditions are placed on the spatial lattice the nucleus "realizes" that the full nuclear wave function "lives" in a much larger space, the "doors are opened wide" and the system "expands" accordingly, until the HFBTHO initial conditions reach in time a complexity comparable to the complexity of the self-consistent many-body wave function obtained on the 3D spatial lattice. We conclude that more accurate initial conditions are needed in the future studies to eliminate the "unphysical" evolution caused by using HFBTHO initial conditions. We remind the reader that we routinely perform (TD)SLDA calculations with a lattice constant $dx = 1$ fm, which corresponds to a cutoff momentum $\Lambda = \hbar\pi/dx \approx 600$ MeV$/c$, which is the typical largest cutoff momentum used in chiral perturbation effective field theory studies of nucleon interactions. It is our hope that by including effective *pn* pairing [11] one can eventually simultaneously capture all long- and short-range correlations in a mean-field-like approach.

The question, however, remains why the actual entropy $S(t)$, the solid and dashed lines in Fig. 12, decreases until scission. The natural explanation is that while the neck is forming, "communication" between the emerging fission fragments is hindered and it completely stops after scission; thus the space in which the quasiparticle wave functions evolve becomes smaller than it was at the initial time. When the neck starts emerging the free flow of nucleons from one side to the other of the elongated nucleus is increasingly inhibited until a time $\approx$700 fm$/c$, when the neck attains a very small diameter and after that the two fission fragments start separating. During this time period until $\approx$700 fm$/c$ the spreading of the single-particle strength is suppressed. After scission the two fission fragments emerge with significant excitation energy, $\approx$15–20 MeV each, but obviously not in thermodynamic equilibrium, as in particular their shapes evolve as well. These aspects are likely also connected with the widely studied problem of many-body localization, a topic of significant interest in predominantly 1D condensed matter systems [84]. When the hopping strength between sites is weaker than the amplitude of the disorder such 1D systems fail to thermalize. The forming of a neck between emerging fission fragments basically plays the same role as disorder in 1D condensed matter systems: it increasingly inhibits the nucleon jumps between these emerging fission fragments. Unlike in the case of a system in contact with a thermostat, the entropy of an isolated many-body system or, in a more precise language, the complexity of its many-body wave function does not necessarily always increase monotonically in time at intermediate times. A similar situation is often used in demonstrations in introductory physics classes: when compressed air is released from a container, it cools, and its entropy decreases.

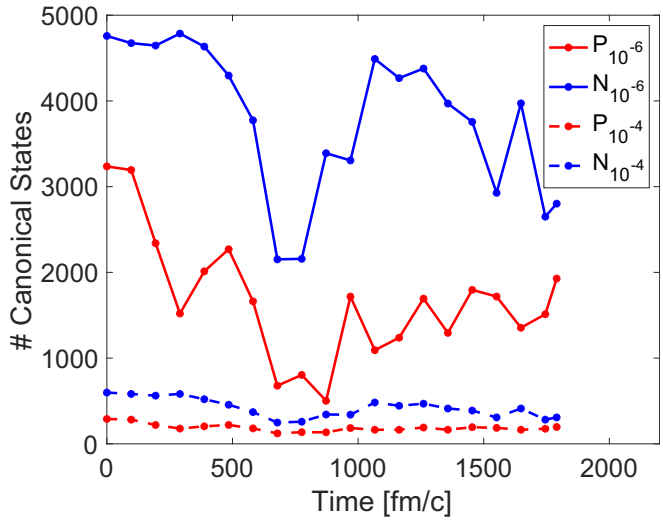

FIG. 13. The number of canonical states vs time for cutoffs $n_k \leqslant 10^{-4}$ and 10^{-6}, respectively. These have to be compared with the size of the entire set of canonical wave functions $2N - xN_yN_z = 108\,000$ in this study.

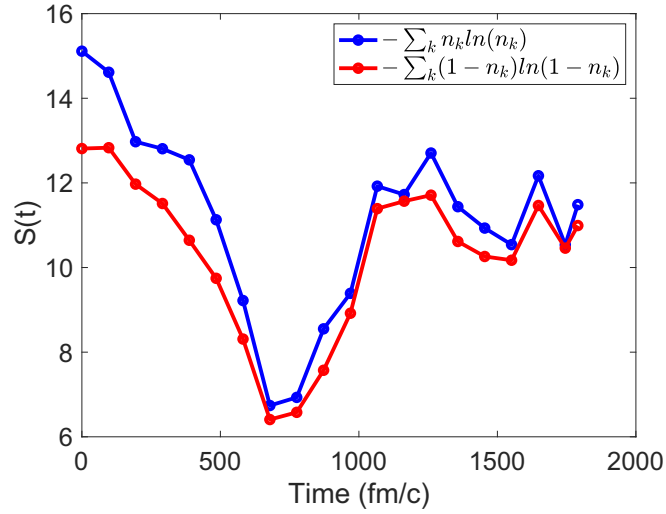

FIG. 14. The time dependence of the two parts of the entanglement entropy $S(t) = S_1(t) + S_2(t)$, where $S_1(t) = -\sum_k n_k \ln n_k$ and $S_2(t) = -\sum_k (1-n_k)\ln(1-n_k)$. Up to an additive constant and an overall normalization, $S_1(t)$ is equal to the Shannon entropy $\overline{S}$ [see Eq. (12)].

It is instructive to determine the number of canonical states with occupation probabilities n_k up to different cutoffs (see Fig. 13). A cutoff in canonical occupation probabilities at the level $n_k \geqslant 10^{-5}$ can be sufficient for evaluating particle number with a relative accuracy $\mathcal{O}(10^{-4})$ (see also Fig. 10). However, for the evaluation of the entanglement entropy, which is a more accurate measure of the complexity of the many-body wave function, a cutoff in $n_k \geqslant 10^{-6}$–10^{-7} is needed (see Fig. 11).

It is also instructive to evaluate the two different contributions to the entanglement entropy $S(t) = S_1(t) + S_2(t)$ [see Eq. (4)]. As one can judge from Fig. 14, $S_1(t)$ and $S_2(t)$ have a very similar behavior and almost equal magnitudes. This is particularly relevant, since $S_1(t)$ is identical to the Shannon entropy $\overline{S}$, up to an additive constant and a multiplicative factor [see Eq. (12)].

One might hastily conclude that our conclusions are limited to the case of pairing correlations only. This conclusion would be wrong for several reasons. First, even when the pairing correlations, not necessarily the pairing condensates, occur only in the s wave between protons and neutrons only, the corresponding pairing fields still describe the role of collisions. At the semiclassical level such collisions are incorporated by the collision integral in the extension of the Boltzmann equation due to Nordheim [98] and Uehling-Uhlenbeck [99] at finite local temperatures (see also the discussion in Ref. [11]). The results obtained so far in the study of numerous cold-atom and nuclear systems amply demonstrate that when these systems are highly excited, well above the critical temperature T_c for the onset of pairing condensates, and their corresponding pairing correlations are absent, the high-momentum states are increasingly occupied as time goes on (see Refs. [93–97]). In the results illustrated in Fig. 14, at times beyond 700 fm/c in the emerging fission fragments pairing condensates are absent and the temperature of the fission fragments is $T > T_c$. Second, in a Kohn-Sham-like extension of the time-dependent DFT (TDDFT) the role of finite-range interactions can be incorporated only through local potentials, as nonlocal Fock-like potentials will not be used in the foreseeable future in time-dependent simulations. For example, in Ref. [36] it is shown how the role of the tensor interaction at high-momentum transfer can be emulated with a pure attractive s-wave interaction in the pn triplet channel, which dominates the SRCs in nuclear systems. Third, note that even in the Boltzmann equation and its semiclassical extension, the Boltzmann-Uehling-Uhlenbeck equation, the collisions are always local in space and describe the time evolution of the one-body density matrix, similarly to TDDFT. Collisions in higher partial waves will likely be incorporated by corresponding anomalous densities depending on various gradients of the quasiparticle wave functions, as is done currently also for the corresponding terms in the self-consistent Skyrme-like potentials. The pn collisions, in particular, play the role of collisions due to the tensor interactions, and are still absent in current nuclear TDSLDA simulations, but they can and will soon be incorporated [11].

In Fig. 12 we show the entanglement entropy evaluated both before and after particle projections. For times larger than 700 fm/c the nuclear system is normal ($T > T_c$), and these entropies increase with time as expected for a nonequilibrium process. The number of Slater determinants in the corresponding particle projected expansion of the highly correlated many-body wave function is still increasing in time. This number can be estimated for either the proton or neutron systems to be on the order of 10^{120}–10^{140} using Eq. (1) with the number of relevant single-particle orbitals extracted from Fig. 13. This estimate is orders of magnitude larger than any size ever attempted in CI calculations, which never take into account explicitly SRCs. As our own still unpublished results in larger spaces confirm, the number of canonical

states and/or natural orbitals in a time-dependent situation increase dramatically with the size of the simulation. As more single-particle states become available the number of accessible final states increases as well and the trajectory of the reaction changes accordingly, as one would naturally expect.

VI. CONCLUSIONS

To study the complexity of a many-fermion wave function we have concentrated here on the properties of the canonical wave functions and/or natural orbitals basis set and the corresponding occupation probabilities. Unlike previous studies, which were limited only to the study of canonical wave functions and/or natural orbitals only for the ground state of various systems and small basis sets of such states, we have extended our analysis to excited and in particular to many-fermion functions describing nonequilibrium processes and have shown that their properties are universal and general properties of the one-body density matrix, whether the system is static or time dependent (see also Refs. [11,138]). The canonical wave functions and/or natural orbitals fall basically into two distinct categories: The first group corresponds to wave functions with their support predominantly inside the nucleus. The second category corresponds to wave functions with their support outside the nucleus, and in the limit of high spatial resolution ($\Lambda \to \infty$) these wave functions have vanishing occupation probabilities and hence do not contribute to observables. We have dubbed these two categories as "interior" and "exterior" canonical wave functions. As far as we are aware, the existence and properties of these two sets of canonical wave functions and/or natural orbitals has not been discussed in literature. The "interior" wave functions fall into two subgroups: the first group corresponding to occupation probabilities described by well-known either Bardeen-Cooper-Schrieffer distribution in the presence of pairing correlations or the textbook distribution [139]

$$n(k) = \frac{1}{1 + \exp[-\beta(\epsilon(k) - \mu)]}, \tag{35}$$

where $\beta = 1/T$, and the second group which has a power-law behavior

$$n(k) = \frac{C}{k^4}, \tag{36}$$

due to SRCs [11,36,37,45–47] in both cold atoms and nuclear systems, in particular due to the dominant role of the tensor interactions between protons and neutrons [21–25,28–44] in nuclear systems. Moreover, while for an isolated quantum system in vacuum the cardinality of the entire set of canonical wave functions is $\mathfrak{c} = |\mathbb{R}^3|$, the cardinality of the "interior" subset of canonical wave functions is only $\aleph_0 = |\mathbb{Z}| = |\mathbb{N}|$. The spatial profile of these "interior" wave functions has the hallmark behavior of "standing waves" in a finite potential well, with their "spatial frequencies" extending up to infinity when $\Lambda \to \infty$. These "interior" states should not be confused with single-particle quantized states, which can be defined only in the case of static HF or HFB calculations, where the (generalized) density matrix commutes with the (generalized) single-body Hamiltonian.

In calculations performed in finite spatial boxes, the set of physically relevant "interior" canonical wave functions only has a significantly smaller size than the full set, which can be crucial in performing many-body simulations within such a reduced space, but "physically complete" set. The set of $-\ln n_k$ is also known as the entanglement spectrum [79] and it is widely used in literature to characterize the properties of strongly interacting many-body systems [80–89].

The canonical basis set appears well suited for performing shell-model calculations [14]. However, it remains a challenge to reformulate TDDFT explicitly within this basis. Approximate sets of canonical states can be easily generated, for example, for nuclear problems, by solving the non-self-consistent equations for the radial wave functions

$$\begin{pmatrix} H - \mu & \Delta \\ \Delta & -H^* + \mu \end{pmatrix} \begin{pmatrix} \mathrm{u}_k \\ \mathrm{v}_k \end{pmatrix} = E_k \begin{pmatrix} \mathrm{u}_k \\ \mathrm{v}_k \end{pmatrix}, \tag{37}$$

$$H = -\frac{\hbar^2 \nabla^2}{2m} + V + V_{so}, \tag{38}$$

where the central potential V and the pairing field Δ have spherical symmetry, and V_{so} is an appropriate single-particle spin-orbit potential. The generation of sufficiently large sets of canonical wave functions, or natural orbitals, with exact quantum numbers $njlm$, in the case of spherical symmetry, is numerically cheap and the set can be adapted for the problems studied in Refs. [61–73]. Unlike the sets of natural orbitals used in these papers and many similar studies in atomic physics and chemistry calculations, the sets we discussed here are accurate, have no negative canonical occupation probabilities, as they should, can be generated easily with the expected spherical symmetry, and their quality can be easily improved during the calculations by adapting the properties of the potentials V, V_{so}, μ, and Δ to ensure high accuracy within a relatively small size basis set. A particular aspect which we observed is that the canonical wave functions $\phi_k(\xi)$ depend very weakly on the magnitude of the pairing field Δ.

Induced nuclear fission and collisions of heavy ions are a particularly relevant highly nonequilibrium strongly interacting quantum many-body system to study. Nuclear fragments emerge highly excited in both fission and heavy-ion collisions, with an average temperature well above the critical temperature $T > T_c$ [11,95,133], at an excitation energy at which the pairing correlations are absent. Therefore, the fact that we formally obtained the result that the final quantum Boltzmann one-body or entanglement entropy increases within a formalism emerging from a treatment of pairing correlations, in particular even after performing a projection on the total proton and neutron numbers, furthermore underlines our conclusion that this increase is indeed solely related to the significant larger degree of complexity and more entanglement in the final many-body wave function compared to the initial many-body function.

Long tails of the momentum distribution have been measured [36,43] and a comprehensive picture of nuclei should and can incorporate both mean-field and SRCs

[11,138]. These conclusions are in full agreement with Tan's [37–39,45–47] conclusion that the presence of SRCs, although not necessarily always with "pure" character $n_k = C/k^4$, are present irrespective of whether the system is superfluid or a Fermi-like liquid. The presence of these long tails for n_k leads to a generalization of the textbook definition [139] of the equilibrium single-particle occupation probabilities in strongly interacting many-fermion systems [138].

As the example of induced fission shows, the current implementation of the extension to superfluid systems of the TDDFT includes single-particle momenta up to ≈600 MeV/c, the upper limit considered in current implementations of the chiral effective field theory for nucleon interactions in the treatment of light, medium, and even heavy nuclei. Upon including the proton-neutron dynamical pairing correlations one would be able to basically describe, within a unified approach, both long-range and short-range nucleon correlations [11], particularly for nonequilibrium processes. The highly nonequilibrium nuclear fission process discussed here is apparently the largest system where quantum entanglement has been studied so far [74–89], with aspects related to the widely studied topics of Hilbert space and many-body localization.

As a result of our present analysis we expect that the properties of the canonical basis set and the use of entanglement entropy can be extended to strongly correlated quantum many-body systems in order to characterize the degree of complexity of the corresponding many-body wave functions and the degree of their entanglement, and thus provide additional insight into the QIS of many-body systems and their dynamics. As a side result, we provided a method to construct easily a set of approximate canonical wave functions and/or natural orbitals with correct quantum numbers, which can be improved while a solution to the many-body problem is constructed.

ACKNOWLEDGMENTS

The funding from the U.S. DOE, Office of Science, Grant No. DE-FG02-97ER41014 and also the support provided in part by NNSA Cooperative Agreement No. DE-NA0003841 is greatly appreciated. This research used resources of the Oak Ridge Leadership Computing Facility, which is a U.S. DOE Office of Science User Facility supported under Contract No. DE-AC05-00OR22725.

APPENDIX

We will review here the Bogoliubov-Valatin formalism and the definition of the canonical wave functions. As Klich [101] has shown, the same formalism can be used to characterize the entanglement entropy of any noninteracting system partitioned into two complementary parts. At the same time the reader should be aware that the definition of the entanglement entropy is not unique, as there are many different way to partition a system into two subsystems and we refer the reader to reviews where these differences have been discussed in rather great detail [102–105].

The creation $\alpha_k^\dagger$ and annihilation α_k quasiparticle operators are represented with a unitary transformation from the field operators as follows [10]:

$$\alpha_k^\dagger = \int d\xi [\mathrm{u}_k(\xi)\psi^\dagger(\xi) + \mathrm{v}_k(\xi)\psi(\xi)], \tag{A1}$$

$$\alpha_k = \int d\xi [\mathrm{v}_k^*(\xi)\psi^\dagger(\xi) + \mathrm{u}_k^*(\xi)\psi(\xi)], \tag{A2}$$

and with the reverse relations

$$\psi^\dagger(\xi) = \sum\!\!\!\!\!\!\int_k [\mathrm{u}_k^*(\xi)\alpha_k^\dagger + \mathrm{v}_k(\xi)\alpha_k], \tag{A3}$$

$$\psi(\xi) = \sum\!\!\!\!\!\!\int_k [\mathrm{v}_k^*(\xi)\alpha_k^\dagger + \mathrm{u}_k(\xi)\alpha_k]. \tag{A4}$$

Here $\psi^\dagger(\xi)$ and $\psi(\xi)$ are the field operators for the creation and annihilation of a particle with coordinate $\xi = (\boldsymbol{r}, \sigma, \tau)$, $(u_k(\xi), v_k(\xi))^T$ are the quasiparticle wave functions, and the integral implies also a summation over discrete variables when appropriate. In a finite volume, with periodic boundary conditions, the index k is always discrete. For a finite isolated system in vacuum [112,140] the sum over k stands for a summation over the discrete indices and an integral over the continuous ones, respectively.

The Hermitian number density and the skew-symmetric anomalous density matrices are defined as

$$n(\xi,\zeta) = \langle\Phi|\psi^\dagger(\zeta)\psi(\xi)|\Phi\rangle = \sum\!\!\!\!\!\!\int_k \mathrm{v}_k^*(\xi)\mathrm{v}_k(\zeta), \tag{A5}$$

$$\overline{n}(\xi,\zeta) = \langle\Phi|\psi(\xi)\psi^\dagger(\zeta)|\Phi\rangle = \sum\!\!\!\!\!\!\int_k \mathrm{u}_k(\xi)\mathrm{u}_k^*(\zeta), \tag{A6}$$

$$\kappa(\xi,\zeta) = \langle\Phi|\psi(\zeta)\psi(\xi)|\Phi\rangle = \sum\!\!\!\!\!\!\int_k \mathrm{v}_k^*(\xi)\mathrm{u}_k(\zeta) \tag{A7}$$

$$n(\xi,\zeta) + \overline{n}(\xi,\zeta) = \delta(\xi-\zeta), \tag{A8}$$

where the quasiparticle vacuum is defined as

$$\alpha_k|\Phi\rangle = 0, \quad |\Phi\rangle = \mathcal{N}\prod_k \alpha_k|0\rangle, \quad \langle\Phi|\alpha_k\alpha_l^\dagger|\Phi\rangle = \delta_{kl}, \tag{A9}$$

and $\mathcal{N}$ is a normalization factor (determined up to an arbitrary phase), $\alpha_k|0\rangle \neq 0$, and $|0\rangle$ is the vacuum state. For any k, if the norm $\int d\xi |\mathrm{v}_k(\xi)|^2 = 0$ the corresponding factor α_k should be skipped in the definition of $|\Phi\rangle$. The new density matrix $\overline{n}(\xi,\zeta)$ is used in the discussion of the canonical basis set.[2]

The anticommutation relations for the field operators $\psi^\dagger(\xi)$, $\psi(\xi)$ and for the quasiparticle operators $\alpha_k^\dagger$, α_k imply that [10]

$$\int d\xi\, [\mathrm{u}_k^*(\xi)\mathrm{u}_l(\xi) + \mathrm{v}_k^*(\xi)\mathrm{v}_l(\xi)] = \delta_{kl}, \tag{A10}$$

$$\int d\xi\, [\mathrm{u}_k(\xi)\mathrm{v}_l(\xi) + \mathrm{v}_k(\xi)\mathrm{u}_l(\xi)]y = 0, \tag{A11}$$

[2]The wave functions $v_k(\xi)$ can be considered either as the vectors labeled by k with components enumerated by ξ or as the vectors labeled by ξ and components enumerated by k. Thus $n(\xi,\zeta)$ is the complex scalar product of vectors with labels ξ and ζ, while $\langle v_k|v_l\rangle$ is the complex scalar product of vectors k and l.

$$\sum\!\!\!\!\!\!\int_k [\mathrm{u}_k(\xi)\mathrm{u}_k^*(\zeta) + \mathrm{v}_k^*(\xi)\mathrm{v}_k(\zeta)] = \delta(\xi - \zeta), \tag{A12}$$

$$\sum\!\!\!\!\!\!\int_k [\mathrm{u}_k(\xi)\mathrm{v}_k^*(\zeta) + \mathrm{v}_k^*(\xi)\mathrm{u}_k(\zeta)] = 0. \tag{A13}$$

Equation (A12) means that the quasiparticle wave functions $\mathrm{u}_k(\xi)$, $\mathrm{v}_k(\xi)$ form (in general) an overcomplete set, as for an arbitrary function $g(\xi)$ one has the decomposition

$$g(\xi) = \sum\!\!\!\!\!\!\int_k \mathrm{u}_k(\xi) \int d\zeta\, \mathrm{u}_k^*(\zeta) g(\zeta) + \sum\!\!\!\!\!\!\int_k \mathrm{v}_k^*(\xi) \int d\zeta\, \mathrm{v}_k(\zeta) g(\zeta). \tag{A14}$$

Additionally one can show that [10]

$$\int d\zeta\, [n(\xi,\zeta)n(\zeta,\eta) + \kappa(\xi,\zeta)\kappa^\dagger(\zeta,\eta)] = n(\xi,\eta), \tag{A15}$$

$$\int d\zeta\, n(\xi,\zeta)\kappa(\zeta,\eta) = \int d\zeta\, \kappa(\xi,\zeta)n^*(\zeta,\eta). \tag{A16}$$

For a finite system the quasiparticle components $\mathrm{v}_k(\xi)$ always have a finite norm [112]

$$\int d\xi\, |\mathrm{v}_k(\xi)|^2 < \infty, \tag{A17}$$

unlike the quasiparticle components $\mathrm{u}_k(\xi)$, which can be either normalizable or not in an infinite volume. The index k can be either discrete or continuous, respectively.

One can consider an arbitrary unitary transformation $\mathcal{U}\mathcal{U}^\dagger = \mathbb{I}$ (where $\mathbb{I}$ is the identity operator) of the quasiparticle wave functions

$$\tilde{\mathrm{v}}_l = \sum\!\!\!\!\!\!\int_k \mathcal{U}_{kl}\mathrm{v}_k, \quad \mathrm{v}_k = \sum\!\!\!\!\!\!\int_l \mathcal{U}_{kl}^*\tilde{\mathrm{v}}_l, \tag{A18}$$

$$\tilde{\mathrm{u}}_l = \sum\!\!\!\!\!\!\int_k \mathcal{U}_{kl}\mathrm{u}_k, \quad \mathrm{u}_k = \sum\!\!\!\!\!\!\int_l \mathcal{U}_{kl}^*\tilde{\mathrm{u}}_l, \tag{A19}$$

which leaves the normal and anomalous density matrices unchanged. This type of transformation for quasiparticle wave functions was suggested in Refs. [123,141] in order to simultaneously diagonalize the overlap matrices $\langle \mathrm{v}_k|\mathrm{v}_l\rangle$ and $\langle \mathrm{u}_k|\mathrm{u}_l\rangle$. Only the canonical occupation probabilities are invariant with respect to arbitrary unitary transformations $\mathcal{U}$ mentioned above and one can then show that

$$n(\xi,\zeta) = \sum\!\!\!\!\!\!\int_k n_k\phi_k^*(\xi)\phi_k(\zeta), \tag{A20}$$

$$\kappa(\xi,\zeta) = \sum\!\!\!\!\!\!\int_k \sqrt{n_k(1-n_k)}\phi_{\bar{k}}^*(\xi)\phi_k(\zeta), \tag{A21}$$

where

$$\phi_{\bar{k}}^*(\xi) = \frac{1}{\sqrt{n_k(1-n_k)}} \int d\zeta\, \kappa(\xi,\zeta)\phi_k^*(\zeta), \tag{A22}$$

$$\langle\phi_k|\phi_{\bar{k}}^*\rangle = 0, \quad \langle\phi_{\bar{k}}^*|\phi_{\bar{k}}^*\rangle = 1, \tag{A23}$$

$$\int d\zeta\, n(\xi,\zeta)\phi_{\bar{k}}^*(\zeta) = n_k\phi_{\bar{k}}^*(\xi), \tag{A24}$$

where only $0 < n_k < 1$ contribute in Eqs. (A21) and (A22) and Eqs. (A23) and (A24) follow from Eqs. (5), (A15), and (A16).

In the Hartree-Fock (HF) approximation the situation is much simpler; since $n_k = 0$ or 1, the anomalous density vanishes and the occupation probabilities are defined in the representation which simultaneously diagonalizes the number density matrix and the mean field, and in that particular representation the occupation probabilities have a straightforward physical interpretation. In the presence of pairing correlations one can introduce a generalized density matrix [10], which commutes with the generalized mean field. However, in that representation the normal number density has the form given by Eq. (A5), where $\langle \mathrm{v}_k|\mathrm{v}_l\rangle \neq n_k\delta_{kl}$. One can define the occupation probabilities either as $n_k = \langle \mathrm{v}_k|\mathrm{v}_k\rangle$ in the representation in which the generalized mean field is diagonal, or instead use the canonical occupation probabilities n_k from Eq. (5) and define the single-particle energies as $e_k = \langle\phi_k|H|\phi_k\rangle$, where H is the normal mean-field single-particle Hamiltonian within the Hartree-Fock-Bogoliubov (HFB) and superfluid local density approximation (SLDA) frameworks, and in which case $\langle\phi_k|H|\phi_l\rangle \neq 0$ if $k \neq l$. The simple relationship between the HF occupation probabilities and the single-particle energies thus becomes more difficult to interpret physically and justify within HFB and SLDA frameworks.[3]

Since the total particle number is not well defined within HFB and SLDA, as the gauge symmetry is broken, one has to restore this symmetry. In the canonical representation the gauge symmetry is significantly easier to restore [123,141]. The many-body wave function acquires the well-known BCS form $|\Phi\rangle = \Pi_k(u_k + v_k a_k^\dagger a_{\bar{k}}^\dagger)|0\rangle$ [6], where $a_k|0\rangle = 0$, $u_k^2 + v_k^2 = 1$, and $n_k = v_k^2$ and various other gauge-symmetry-restored observables can be easily extracted [123].

The quasiparticle representation in which the generalized number density matrix and the generalized mean field commute is particularly suited for numerically determining the corresponding static many-body wave function $|\Phi\rangle$, only if one uses diagonalization methods. The diagonalization, which is typically numerically very expensive, can be eschewed [142], as both normal and anomalous densities can be determined without the knowledge of the quasiparticle wave functions (qpwfs) and of the corresponding quasiparticle energies.

[3]Any many-fermion system, either superfluid or normal, can be described using the same formalism, as one can introduce a normal number density matrix [Eq. (A20)] and an "anomalous number density" [Eq. (A21)] with the functions $v_k(\xi) = \sqrt{n_k}\phi_k(\xi)$ and $u_k(\xi) = \sqrt{1-n_k}\phi_{\bar{k}}(\xi)$ [101].

[1] E. Schrödinger, An undulatory theory of the mechanics of atoms and molecules, Phys. Rev. **28**, 1049 (1926).

[2] D. R. Hartree, The wave mechanics of an atom with a non-Coulomb central field. Part II. Some results and discussion, Math. Proc. Cambridge Philos. Soc. **24**, 111 (1928).

[3] J. C. Slater, The self consistent field and the structure of atoms, Phys. Rev. **32**, 339 (1928).

[4] J. C. Slater, Note on Hartree's method, Phys. Rev. **35**, 210 (1930).

[5] V. Fock, Näherungsmethode zur Lösung des quantenmechanischen Mehrkörperproblems, Z. Phys. **61**, 126 (1930).

[6] J. Bardeen, L. N. Cooper, and J. R. Schrieffer, Theory of superconductivity, Phys. Rev. **108**, 1175 (1957).

[7] N. N. Bogoljubov, On a new method in the theory of superconductivity, Il Nuovo Cimento **7**, 794 (1958).

[8] J. G. Valatin, Comments on the theory of superconductivity, Il Nuovo Cimento **7**, 843 (1958).

[9] P. G. De Gennes, *Superconductivity of Metals and Alloys* (CRC Press, Boca Raton, FL, 1999).

[10] P. Ring and P. Schuck, *The Nuclear Many-Body Problem*, 1st ed. (Springer-Verlag, Berlin, 2004).

[11] A. Bulgac, Pure quantum extension of the semiclassical Boltzmann-Uehling-Uhlenbeck equation, Phys. Rev. C **105**, L021601 (2022).

[12] A. Bohr and B. R. Mottelson, *Nuclear Structure* (Benjamin, New York, 1969), Vol. I.

[13] P. A. Anderson, *Basic Notions of Condensed Matter Physics* (Benjamin Cummings, London, 1984).

[14] C. W. Johnson, Current status of very-large-basis Hamiltonian diagonalizations for nuclear physics, arXiv:1809.07869

[15] P.-O. Löwdin, Quantum theory of cohesive properties of solids, Adv. Phys. **5**, 1 (1956).

[16] P.-O. Löwdin and H. Shull, Natural orbitals in the quantum theory of two-electron systems, Phys. Rev. **101**, 1730 (1956).

[17] A. J. Coleman, Structure of fermion density matrices, Rev. Mod. Phys. **35**, 668 (1963).

[18] A. J. Coleman, Discussion on "Structure of fermion density matrices", Rev. Mod. Phys. **35**, 687 (1963).

[19] E. R. Davidson, Properties and uses of natural orbitals, Rev. Mod. Phys. **44**, 451 (1972).

[20] J. S. Levinger, The high energy nuclear photoeffect, Phys. Rev. **84**, 43 (1951).

[21] O. Benhar, V. R. Pandharipande, and S. C. Pieper, Electron-scattering studies of correlations in nuclei, Rev. Mod. Phys. **65**, 817 (1993).

[22] V. R. Pandharipande, I. Sick, and P. K. A. de Witt Huberts, Independent particle motion and correlations in fermion systems, Rev. Mod. Phys. **69**, 981 (1997).

[23] E. N. M. Quint, J. F. J. van den Brand, J. W. A. den Herder, E. Jans, P. H. M. Keizer, L. Lapikás, G. van der Steenhoven, P. K. A. de Witt Huberts, S. Klein, P. Grabmayr, G. J. Wagner, H. Nann, B. Frois, and D. Goutte, Relative $3s$ Spectroscopic Strength in ^{206}Pb and ^{208}Pb Studied with the $(e, e'p)$ Knockout Reaction, Phys. Rev. Lett. **57**, 186 (1986).

[24] E. N. M. Quint, B. M. Barnett, A. M. van den Berg, J. F. J. van den Brand, H. Clement, R. Ent, B. Frois, D. Goutte, P. Grabmayr, J. W. A. den Herder, E. Jans, G. J. Kramer, J. B. J. M. Lanen, L. Lapikás, H. Nann, G. van der Steenhoven, G. J. Wagner, and P. K. A. de Witt Huberts, Evidence for Partial Occupancy of the $3s_{1/2}$ Proton Orbit in ^{208}Pb, Phys. Rev. Lett. **58**, 1088 (1987).

[25] T. Aumann, C. Barbieri, D. Bazin, C.A. Bertulani, A. Bonaccorso, W.H. Dickhoff, A. Gade, M. Gómez-Ramos, B.P. Kay, A.M. Moro, T. Nakamura, A. Obertelli, K. Ogata, S. Paschalis, and T. Uesaka, Quenching of single-particle strength from direct reactions with stable and rare-isotope beams, Prog. Part. Nucl. Phys. **118**, 103847 (2021).

[26] B. D. Day, Elements of the Brueckner-Goldstone theory of nuclear matter, Rev. Mod. Phys. **39**, 719 (1967).

[27] J. W. Negele, The mean-field theory of nuclear structure and dynamics, Rev. Mod. Phys. **54**, 913 (1982).

[28] R. Sartor and C. Mahaux, Self-energy, momentum distribution, and effective masses of a dilute Fermi gas, Phys. Rev. C **21**, 1546 (1980).

[29] L. L. Frankfurt and M. I. Strikman, High-energy phenomena, short-range nuclear structure and QCD, Phys. Rep. **76**, 215 (1981).

[30] L. Frankfurt and M. Strikman, Hard nuclear processes and microscopic nuclear structure, Phys. Rep. **160**, 235 (1988).

[31] C. Ciofi degli Atti and S. Simula, Realistic model of the nucleon spectral function in few- and many-nucleon systems, Phys. Rev. C **53**, 1689 (1996).

[32] E. Piasetzky, M. Sargsian, L. Frankfurt, M. Strikman, and J. W. Watson, Evidence for Strong Dominance of Proton-Neutron Correlations in Nuclei, Phys. Rev. Lett. **97**, 162504 (2006).

[33] M. M. Sargsian, T. V. Abrahamyan, M. I. Strikman, and L. L. Frankfurt, Exclusive electrodisintegration of ^{3}He at high Q^2. II. Decay function formalism, Phys. Rev. C **71**, 044615 (2005).

[34] R. Schiavilla, R. B. Wiringa, S. C. Pieper, and J. Carlson, Tensor Forces and the Ground-State Structure of Nuclei, Phys. Rev. Lett. **98**, 132501 (2007).

[35] M. M. Sargsian, New properties of the high-momentum distribution of nucleons in asymmetric nuclei, Phys. Rev. C **89**, 034305 (2014).

[36] O. Hen, G. A. Miller, E. Piasetzky, and L. B. Weinstein, Nucleon-nucleon correlations, short-lived excitations, and the quarks within, Rev. Mod. Phys. **89**, 045002 (2017).

[37] *The BCS-BEC Crossover and the Unitary Fermi Gas*, edited by W. Zwerger, Lecture Notes in Physics Vol. 836 (Springer-Verlag, Berlin, 2012).

[38] E. Braaten, Universal relations for fermions with large scattering length, in *The BCS-BEC Crossover and the Unitary Fermi Gas* (Springer, Berlin, 2012), Chap. 6, pp. 193–231.

[39] Y. Castin and F. Werner, The unitary gas and its symmetry properties, in *The BCS-BEC Crossover and the Unitary Fermi Gas* (Springer, Berlin, 2012), Chap. 5.

[40] E. R. Anderson and J. E. Drut, Pressure, Compressibility, and Contact of the Two-Dimensional Attractive Fermi Gas, Phys. Rev. Lett. **115**, 115301 (2015).

[41] W. J. Porter and J. E. Drut, Tan's contact and the phase distribution of repulsive Fermi gases: Insights from quantum chromodynamics noise analyses, Phys. Rev. A **95**, 053619 (2017).

[42] J. T. Stewart, J. P. Gaebler, T. E. Drake, and D. S. Jin, Verification of Universal Relations in a Strongly Interacting Fermi Gas, Phys. Rev. Lett. **104**, 235301 (2010).

[43] O. Hen *et al.*, Momentum sharing in imbalanced Fermi systems, Science **346**, 614 (2014).

[44] R. Cruz-Torres, D. Lonardoni, R. Weiss, M. Piarulli, N. Barnea, D. W. Higinbotham, E. Piasetzky, A. Schmidt, L. B. Weinstein, R. B. Wiringa, and O. Hen, Many-body factorization and position-momentum equivalence of nuclear short-range correlations, Nat. Phys. **17**, 306 (2021).

[45] S. Tan, Energetics of a strongly correlated Fermi gas, Ann. Phys. **323**, 2952 (2008).

[46] S. Tan, Large momentum part of a strongly correlated Fermi gas, Ann. Phys. **323**, 2971 (2008).

[47] S. Tan, Generalized virial theorem and pressure relation for a strongly correlated Fermi gas, Ann. Phys. **323**, 2987 (2008).

[48] S. K. Bogner, R. J. Furnstahl, and A. Schwenk, From low-momentum interactions to nuclear structure, Prog. Part. Nucl. Phys. **65**, 94 (2010).

[49] R. J. Furnstahl and K. Hebeler, New applications of renormalization group methods in nuclear physics, Rep. Prog. Phys. **76**, 126301 (2013).

[50] A. J. Tropiano, S. K. Bogner, and R. J. Furnstahl, Short-range correlation physics at low renormalization group resolution, Phys. Rev. C **104**, 034311 (2021).

[51] A. J. Tropiano, S. K. Bogner, R. J. Furnstahl, and M. A. Hisham, Quasi-deuteron model at low renormalization group resolution, Phys. Rev. C **106**, 024324 (2022).

[52] B. Hu, W. Jiang, T. Miyagi, Z. Sun, A. Ekström, C. Forssén, G. Hagen, J. D. Holt, T. Papenbrock, S. R. Stroberg, and I. Vernon, Ab initio predictions link the neutron skin of ^{208}Pb to nuclear forces, Nat. Phys. **18**, 1196 (2022).

[53] P. Maris *et al.* (LENPIC Collaboration), Light nuclei with semilocal momentum-space regularized chiral interactions up to third order, Phys. Rev. C **103**, 054001 (2021).

[54] I. Tews *et al.*, Nuclear forces for precision nuclear physics: A collection of perspectives, Few-Body Syst. **63**, 67 (2022).

[55] A. Sorensen *et al.*, Dense nuclear matter equation of state from heavy-ion collisions, arXiv:2301.13253.

[56] G. A. Miller, Discovery versus precision in nuclear physics: A tale of three scales, Phys. Rev. C **102**, 055206 (2020).

[57] G. A. Miller, A. Beck, S. May-Tal Beck, L. B. Weinstein, E. Piasetzky, and O. Hen, Can long-range nuclear properties be influenced by short range interactions? A chiral dynamics estimate, Phys. Lett. B **793**, 360 (2019).

[58] B. Zumino, Normal forms of complex matrices, J. Math. Phys. **3**, 1055 (1962).

[59] C. Bloch and A. Messiah, The canonical form of an antisymmetric tensor and its application to the theory of superconductivity, Nucl. Phys. **39**, 95 (1962).

[60] V. R. Pandharipande, C. N. Papanicolas, and J. Wambach, Occupation Probabilities of Shell-Model Orbits in the Lead Region, Phys. Rev. Lett. **53**, 1133 (1984).

[61] M. V. Stoitsov, A. N. Antonov, and S. S. Dimitrova, Natural orbital representation and short-range correlations in nuclei, Phys. Rev. C **48**, 74 (1993).

[62] P.-G. Reinhard, M. Bender, K. Rutz, and J. A. Maruhn, An HFB scheme in natural orbitals, Z. Phys. A **358**, 277 (1997).

[63] J. Dobaczewski, W. Nazarewicz, T. R. Werner, J. F. Berger, C. R. Chinn, and J. Dechargé, Mean-field description of ground-state properties of drip-line nuclei: Pairing and continuum effects, Phys. Rev. C **53**, 2809 (1996).

[64] N. Tajima, Canonical-basis solution of the Hartree-Fock-Bogoliubov equation on a three-dimensional Cartesian mesh, Phys. Rev. C **69**, 034305 (2004).

[65] A. Tichai, J. Müller, K. Vobig, and R. Roth, Natural orbitals for *ab initio* no-core shell model calculations, Phys. Rev. C **99**, 034321 (2019).

[66] C. Robin, M. J. Savage, and N. Pillet, Entanglement rearrangement in self-consistent nuclear structure calculations, Phys. Rev. C **103**, 034325 (2021).

[67] J. Hoppe, A. Tichai, M. Heinz, K. Hebeler, and A. Schwenk, Natural orbitals for many-body expansion methods, Phys. Rev. C **103**, 014321 (2021).

[68] P. J. Fasano, C. Constantinou, M. A. Caprio, P. Maris, and J. P. Vary, Natural orbitals for the *ab initio* no-core configuration interaction approach, Phys. Rev. C **105**, 054301 (2022).

[69] M. Chen, T. Li, B. Schuetrumpf, P.-G. Reinhard, and W. Nazarewicz, Three-dimensional Skyrme Hartree-Fock-Bogoliubov solver in coordinate-space representation, Comput. Phys. Commun. **276**, 108344 (2022).

[70] B. S. Hu, J. Padua-Argüelles, S. Leutheusser, T. Miyagi, S. R. Stroberg, and J. D. Holt, *Ab Initio* Structure Factors for Spin-Dependent Dark Matter Direct Detection, Phys. Rev. Lett. **128**, 072502 (2022).

[71] G. Hagen, S. J. Novario, Z. H. Sun, T. Papenbrock, G. R. Jansen, J. G. Lietz, T. Duguet, and A. Tichai, Angular-momentum projection in coupled-cluster theory: Structure of ^{34}Mg, Phys. Rev. C **105**, 064311 (2022).

[72] M. Kortelainen, Z. Sun, G. Hagen, W. Nazarewicz, T. Papenbrock, and P.-G. Reinhard, Universal trend of charge radii of even-even Ca-Zn nuclei, Phys. Rev. C **105**, L021303 (2022).

[73] A. Tichai, S. Knecht, A. T. Kruppa, Ö. Legeza, C. P. Moca, A. Schwenk, M. A. Werner, and G. Zarand, Combining the in-medium similarity renormalization group with the density matrix renormalization group: Shell structure and information entropy, arXiv:2207.01438.

[74] G. J. Milburn, J. Corney, E. M. Wright, and D. F. Walls, Quantum dynamics of an atomic Bose-Einstein condensate in a double-well potential, Phys. Rev. A **55**, 4318 (1997).

[75] G. Vidal, J. I. Latorre, E. Rico, and A. Kitaev, Entanglement in Quantum Critical Phenomena, Phys. Rev. Lett. **90**, 227902 (2003).

[76] V. E. Korepin, Universality of Entropy Scaling in One Dimensional Gapless Models, Phys. Rev. Lett. **92**, 096402 (2004).

[77] A. Kitaev and J. Preskill, Topological Entanglement Entropy, Phys. Rev. Lett. **96**, 110404 (2006).

[78] M. Levin and X.-G. Wen, Detecting Topological Order in a Ground State Wave Function, Phys. Rev. Lett. **96**, 110405 (2006).

[79] H. Li and F. D. M. Haldane, Entanglement Spectrum as a Generalization of Entanglement Entropy: Identification of Topological Order in Non-Abelian Fractional Quantum Hall Effect States, Phys. Rev. Lett. **101**, 010504 (2008).

[80] M. Chuchem, K. Smith-Mannschott, M. Hiller, T. Kottos, A. Vardi, and D. Cohen, Quantum dynamics in the bosonic Josephson junction, Phys. Rev. A **82**, 053617 (2010).

[81] A. Pal and D. A. Huse, Many-body localization phase transition, Phys. Rev. B **82**, 174411 (2010).

[82] J. H. Bardarson, F. Pollmann, and J. E. Moore, Unbounded Growth of Entanglement in Models of Many-Body Localization, Phys. Rev. Lett. **109**, 017202 (2012).

[83] D. Cohen, V. I. Yukalov, and K. Ziegler, Hilbert-space localization in closed quantum systems, Phys. Rev. A **93**, 042101 (2016).

[84] D. A. Abanin, E. Altman, I. Bloch, and M. Serbyn, Colloquium: Many-body localization, thermalization, and entanglement, Rev. Mod. Phys. **91**, 021001 (2019).

[85] S. Sinha and S. Sinha, Chaos and Quantum Scars in Bose-Josephson Junction Coupled to a Bosonic Mode, Phys. Rev. Lett. **125**, 134101 (2020).

[86] S. Wimberger, G. Manganelli, A. Brollo, and L. Salasnich, Finite-size effects in a bosonic Josephson junction, Phys. Rev. A **103**, 023326 (2021).

[87] Q. Liu and K. Ziegler, Entanglement transition through Hilbert-space localization, Phys. Rev. A **107**, 012413 (2023).

[88] N. Mueller, T. V. Zache, and R. Ott, Thermalization of Gauge Theories from their Entanglement Spectrum, Phys. Rev. Lett. **129**, 011601 (2022).

[89] J. T. Schneider, S. J. Thomson, and L. Sanchez-Palencia, Entanglement spectrum and quantum phase diagram of the long-range XXZ chain, Phys. Rev. B **106**, 014306 (2022).

[90] P. Calabrese and J. Cardy, Evolution of entanglement entropy in one-dimensional systems, J. Stat. Mech. (2005) P04010.

[91] P. Calabrese and J. Cardy, Time Dependence of Correlation Functions Following a Quantum Quench, Phys. Rev. Lett. **96**, 136801 (2006).

[92] V. Alba and P. Calabrese, Entanglement and thermodynamics after a quantum quench in integrable systems, Proc. Natl. Acad. Sci. USA **114**, 7947 (2017).

[93] A. Bulgac, Y.-L. Luo, P. Magierski, K. J. Roche, and Y. Yu, Real-time dynamics of quantized vortices in a unitary Fermi superfluid, Science **332**, 1288 (2011).

[94] A. Bulgac and S. Jin, Dynamics of Fragmented Condensates and Macroscopic Entanglement, Phys. Rev. Lett. **119**, 052501 (2017).

[95] A. Bulgac, S. Jin, K. J. Roche, N. Schunck, and I. Stetcu, Fission dynamics of ^{240}Pu from saddle to scission and beyond, Phys. Rev. C **100**, 034615 (2019).

[96] A. Bulgac, S. Jin, and I. Stetcu, Nuclear fission dynamics: Past, present, needs, and future, Front. Phys. **8**, 63 (2020).

[97] P. Magierski, A. Makowski, M. C. Barton, K. Sekizawa, and G. Wlazłowski, Pairing dynamics and solitonic excitations in collisions of medium-mass, identical nuclei, Phys. Rev. C **105**, 064602 (2022).

[98] L. W. Nordheim, On the kinetic method in the new statistics and its application in the electron theory of conductivity, Proc. R. Soc. London A **119**, 689 (1928).

[99] E. A. Uehling and G. E. Uhlenbeck, Transport phenomena in Einstein-Bose and Fermi-Dirac gases. I, Phys. Rev. **43**, 552 (1933).

[100] A. Bulgac, Time-dependent density functional theory and the real-time dynamics of Fermi superfluids, Annu. Rev. Nucl. Part. Sci. **63**, 97 (2013).

[101] I. Klich, Lower entropy bounds and particle number fluctuations in a Fermi sea, J. Phys. A: Math. Gen. **39**, L85 (2006).

[102] L. Amico, R. Fazio, A. Osterloh, and V. Vedral, Entanglement in many-body systems, Rev. Mod. Phys. **80**, 517 (2008).

[103] R. Horodecki, P. Horodecki, M. Horodecki, and K. Horodecki, Quantum entanglement, Rev. Mod. Phys. **81**, 865 (2009).

[104] M. Haque, O. S. Zozulya, and K. Schouten, Entanglement between particle partitions in itinerant many-particle states, J. Phys. A: Math. Theor. **42**, 504012 (2009).

[105] J. Eisert, M. Cramer, and M. B. Plenio, Colloquium: Area laws for the entanglement entropy, Rev. Mod. Phys. **82**, 277 (2010).

[106] K. Boguslawski and P. Tecmer, Orbital entanglement in quantum chemistry, Int. J. Quantum Chem. **115**, 1289 (2015).

[107] N. Gigena and R. Rossignoli, Entanglement in fermion systems, Phys. Rev. A **92**, 042326 (2015).

[108] I. Bengtsson and K. Życzkowski, *Geometry of Quantum States: An Introduction to Quantum Entanglement*, 2nd ed. (Cambridge University Press, Cambridge, UK, 2017).

[109] M. Srednicki, Entropy and Area, Phys. Rev. Lett. **71**, 666 (1993).

[110] A. Bulgac, Local-density-functional theory for superfluid fermionic systems: The unitary Fermi gas, Phys. Rev. A **76**, 040502(R) (2007).

[111] A. Bulgac and M. M. Forbes, Use of the discrete variable representation basis in nuclear physics, Phys. Rev. C **87**, 051301(R) (2013).

[112] A. Bulgac, Hartree-Fock-Bogoliubov approximation for finite systems, arXiv:nucl-th/9907088.

[113] P. Zanardi, Quantum entanglement in fermionic lattices, Phys. Rev. A **65**, 042101 (2002).

[114] Y. Shi, Quantum entanglement of identical particles, Phys. Rev. A **67**, 024301 (2003).

[115] R. Lo Franco and G. Compagno, Quantum entanglement of identical particles by standard information-theoretic notions, Sci. Rep. **6**, 20603 (2016).

[116] F. Benatti, R. Floreanini, F. Franchini, and U. Marzolino, Entanglement in indistinguishable particle systems, Phys. Rep. **878**, 1 (2020).

[117] T. J. F. Johann and U. Marzolino, Locality and entanglement of indistinguishable particles, Sci. Rep. **11**, 15478 (2021).

[118] P. Hohenberg and W. Kohn, Inhomogeneous electron gas, Phys. Rev. **136**, B864 (1964).

[119] R. M. Dreizler and E. K. U. Gross, *Density Functional Theory: An Approach to the Quantum Many-Body Problem* (Springer-Verlag, Berlin, 1990).

[120] *Time-Dependent Density Functional Theory*, edited by M. A. L. Marques, C. A. Ullrich, F. Nogueira, A. Rubio, K. Burke, and E. K. U. Gross, Lecture Notes in Physics Vol. 706 (Springer-Verlag, Berlin, 2006).

[121] *Fundamentals of Time-Dependent Density Functional Theory*, edited by M. A. L. Marques, N. T. Maitra, F. M. S. Nogueira, E. K. U. Gross, and A. Rubio, Lecture Notes in Physics Vol. 837 (Springer, Heidelberg, 2012).

[122] A. Bulgac and M. M. Forbes, Time-dependent density functional theory, in *Energy Density Functional Methods for Atomic Nuclei*, edited by N. Schunck (IOP Publishing, Bristol, UK, 2019), Chap. 4, pp. 4-1–4-34.

[123] A. Bulgac, Restoring broken symmetries for nuclei and reaction fragments, Phys. Rev. C **104**, 054601 (2021).

[124] A. Del Maestro, H. Barghathi, and B. Rosenow, Equivalence of spatial and particle entanglement growth after a quantum quench, Phys. Rev. B **104**, 195101 (2021).

[125] A. Del Maestro, H. Barghathi, and B. Rosenow, Measuring postquench entanglement entropy through density correlations, Phys. Rev. Res. **4**, L022023 (2022).

[126] M. Thamm, H. Radhakrishnan, H. Barghathi, B. Rosenow, and A. Del Maestro, One-particle entanglement for one-dimensional spinless fermions after an interaction quantum quench, Phys. Rev. B **106**, 165116 (2022).

[127] A. Bulgac and Y. Yu, Renormalization of the Hartree-Fock-Bogoliubov Equations in the Case of a Zero Range Pairing Interaction, Phys. Rev. Lett. **88**, 042504 (2002).

[128] A. Bulgac, Local density approximation for systems with pairing correlations, Phys. Rev. C **65**, 051305(R) (2002).

[129] A. Bulgac, Time-dependent density functional theory for fermionic superfluids: From cold atomic gases, to nuclei and neutron star crust, Phys. Status Solidi B **256**, 1800592 (2019).

[130] A. Bulgac, M. M. Forbes, S. Jin, R. Navarro Perez, and N. Schunck, Minimal nuclear energy density functional, Phys. Rev. C **97**, 044313 (2018).

[131] S. Jin, K. J. Roche, I. Stetcu, I.Abdurrahman, and A. Bulgac, The LISE package: Solvers for static and time-dependent superfluid local density approximation equations in three dimensions, Comput. Phys. Commun. **269**, 108130 (2021).

[132] M. Brack and R. K. Bhaduri, *Semiclassical Physics* (Addison-Wesley, Reading, MA, 1997).

[133] A. Bulgac, P. Magierski, K. J. Roche, and I. Stetcu, Induced Fission of ^{240}Pu within a Real-Time Microscopic Framework, Phys. Rev. Lett. **116**, 122504 (2016).

[134] A. Bulgac, I. Abdurrahman, S. Jin, K. Godbey, N. Schunck, and I. Stetcu, Fission Fragment Intrinsic Spins and Their Correlations, Phys. Rev. Lett. **126**, 142502 (2021).

[135] A. Bulgac, I. Abdurrahman, K. Godbey, and I. Stetcu, Fragment Intrinsic Spins and Fragments' Relative Orbital Angular Momentum in Nuclear Fission, Phys. Rev. Lett. **128**, 022501 (2022).

[136] R. Navarro Perez, N. Schunck, R.-D. Lasseri, C. Zhang, and J. Sarich, Axially deformed solution of the Skyrme-Hartree-Fock-Bogolyubov equations using the transformed harmonic oscillator basis (III) HFBHTO (v3.00): A new version of the program, Comput. Phys. Commun. **220**, 363 (2017).

[137] P. Marević, N. Schunck, E. M. Ney, R. Navarro Pérez, M. Verriere, and J. O'Neal, Axially-deformed solution of the Skyrme-Hartree-Fock-Bogoliubov equations using the transformed harmonic oscillator basis (IV) HFBTHO (v4.0): A new version of the program, Comput. Phys. Commun. **276**, 108367 (2022).

[138] A. Bulgac, Entropy, single-particle occupation probabilities, and short-range correlations, arXiv:2203.12079.

[139] A. A. Abrikosov, L. P. Gorkov, and I. E. Dzyaloshinski, *Methods of Quantum Field Theory in Statistical Physics* (Prentice-Hall, Englewood Cliffs, NJ, 1963).

[140] S. T. Belyaev, A. V. Smirnov, S. V. Tolokonnikov, and S. A. Fayans, Pairing in nuclei in the coordinate representation, Sov. J. Nucl. Phys. **45**, 783 (1987).

[141] A. Bulgac, Projection of good quantum numbers for reaction fragments, Phys. Rev. C **100**, 034612 (2019).

[142] S. Jin, A. Bulgac, K. Roche, and G. Wlazłowski, Coordinate-space solver for superfluid many-fermion systems with the shifted conjugate-orthogonal conjugate-gradient method, Phys. Rev. C **95**, 044302 (2017).